THE ASTROPHYSICAL JOURNAL, 216:108–122, 1977 August 15

A SURVEY OF SOFT X-RAY LIMB FLARE IMAGES: THE RELATION BETWEEN THEIR STRUCTURE IN THE CORONA AND OTHER PHYSICAL PARAMETERS

R. PALLAVICINI,* S. SERIO,† AND G. S. VAIANA†
Center for Astrophysics, Harvard College Observatory and Smithsonian Astrophysical Observatory
Received 1976 November 22

ABSTRACT

A survey of soft X-ray limb flare images obtained by the S-054 experiment on board *Skylab* is presented. From a morphological point of view, limb flares have been subdivided into three groups: (A) flares characterized by compact loop structures; (B) flares with a pointlike appearance; (C) flares with large and diffuse systems of loops. The significance of this subdivision is investigated with the aid of plasma parameters determined by combining the S-054 spatially resolved observations with full-disk data obtained by the *Solrad 9* satellite. From a comparison of the spatial structure with physical parameters such as height, volume, energy density, and characteristic times, and from the correlation with white-light coronal transients and Hα active prominences, the existence of two physically distinct classes of flares is established: class I, which consists of both morphological groups A and B, and class II, which comprises only events of group C.

Events of class I are compact flares with smaller volume ($\sim 10^{26}$–10^{27} cm^3) and lower height ($\lesssim 10^4$ km); faster rise and decay times, and shorter duration (~tens of minutes). They have higher energy density ($\sim 10^2$–10^3 ergs cm^{-3}), do not appear to be associated with white-light coronal transients, and are located very low at the base of active regions; their entire structure is bright, with a tendency to be brighter in the lower sections. Events of class II are long-enduring events (~hours) with longer rise and decay times and greater height ($\sim 5 \times 10^4$ km). They have larger volume ($\sim 10^{28}$–10^{29} cm^3) and lower energy density (10–10^2 ergs cm^{-3}) and are associated with prominence eruption or activation and with white-light coronal transients. The large and diffuse systems of loops characteristic of these events are generally brighter at the top.

A model is proposed which qualitatively accounts for the observed differences between the two classes of flares. In particular, it is suggested that compact flares of class I are loops filled from below by evaporated chromospheric material, while flares of class II are probably produced by direct heating of cool condensed material present at coronal heights in the form of a prominence.

Subject headings: Sun: corona — Sun: flares: — Sun: X-rays

I. INTRODUCTION

As a consequence of the *Skylab* mission in 1973–1974, our knowledge of the spatial structure and temporal evolution of soft X-ray flares has substantially increased in comparison with what was known from the few spatially resolved observations obtained before *Skylab* (Vaiana *et al.* 1968; Vaiana and Giacconi 1969; Beigman *et al.* 1969; Vaiana, Krieger, and Timothy 1973; Neupert, Thomas, and Chapman 1974). The physical processes which occur in solar flares, namely, processes of energy deposition and dissipation, depend on the local properties of the plasma and can therefore be adequately investigated only by means of a detailed determination of the local physical conditions. The large number of data obtained in the past years by means of full-disk detectors, although invaluable from a descriptive point of view, have thus revealed themselves as elusive in regard to the solution of quantitative problems. The lack of spatial resolution necessitated the use of physical parameters pertinent to bulk values and independent of the spatial extent of the region, and the neglect of other parameters, such as, for instance, the energy density, knowledge of which is essential for a detailed consideration of the energy deposition and dissipation problem.

Several authors have recently discussed the high-resolution data obtained from *Skylab*. Soft X-ray images of flares observed by the S-054 experiment have been analyzed by Kahler, Krieger, and Vaiana (1975), Petrasso *et al.* (1975), and Pallavicini *et al.* (1975). Observations of flares from a somewhat similar experiment (S-056) on *Skylab* have been presented by Vorpahl *et al.* (1975) and Vorpahl (1976). The relationship between the high-temperature plasma and the cooler transition-region and chromospheric plasma has been investigated by Widing and Cheng (1974), Widing (1975), and Cheng and Widing (1975), using UV data. Pallavicini and Vaiana (1976) and Kundu, Alissandrakis, and Kahler (1976) have performed a comparison between spatially resolved microwave observations and soft X-ray images of flares.

* Osservatorio Astrofisico di Arcetri, Florence, Italy.
† Osservatorio Astrofisico di Palermo, Italy.

These observations have shown that the basic geometrical configuration of the high-temperature flare is represented by one or more filamentary structures whose ends are anchored in regions of opposite magnetic polarity, where the chromospheric Hα emission appears enhanced. These filamentary structures are currently interpreted as loops seen in projection against the solar disk. It has been suggested that small pointlike features ($< 10''$) observed in soft X-ray images are small loops not resolved by the telescope (Vorpahl *et al.* 1975; Kahler, Petrasso, and Kane 1976).

Most of these reported observations relate to flares observed on the disk. In this case the vertical structure of the region lies at least partially along the line of sight; rather than being directly observed, it must be deduced on the basis of plausibility arguments and analogy with a variety of other looplike structures observed both in active and quiet regions of the X-ray Sun. In this paper we shall present images of X-ray flares observed at the solar limb by the S-054 telescope aboard *Skylab*. The direct and obvious aim of this analysis is to test the correctness of the interpretation of disk observations and to obtain confidence in it by comparing events on the disk with events observed at the limb. More important, our analysis allows new physical insights into the mechanisms of solar flares by studying the distribution with height of the emitting plasma and its location with respect to the overall structure of active regions.

Apart from an early observation of a flare near the limb by Krieger, Vaiana, and Van Speybroeck (1971) with a rocket flight, soft X-ray limb flares were briefly discussed in a paper by Vorpahl *et al.* (1975), and a few UV limb events were studied by Widing (1975) and Cheng and Widing (1975). Recently a survey of limb flare observations obtained by the MSFC–Aerospace S-056 experiment on board *Skylab* has been presented by Gibson (1976). There is only a partial overlap of our and Aerospace's data samples. The total number of events selected by us is larger by almost a factor of 2 than in Gibson's paper, even though the criterion we have followed with regard to the position of the events is stricter than Gibson's (we consider limb flares to be only those events with heliographic longitude greater than or equal to 70°, while Gibson includes events at longitude greater than or equal to 64°). Moreover, while all except one of Gibson's flares are smaller than M1 (*Solrad* classification of importance; see following section), we cover a larger range of intensities from subflares of importance less than C1 up to the biggest flares of importance greater than X1. More important, we have concentrated our attention principally on the relationship between the observed spatial structure and the physical parameters of the emitting plasma (trying to understand the physics of the thermal processes of energy deposition and dissipation), while Gibson was more concerned with tracing the structure of the magnetic field from the morphological appearance of the X-ray region (looking for indications about the mechanism of energy storage and the type of instability which triggers the process). This difference in approach has resulted in a different focus of the two papers and in substantial differences in the conclusions, as will appear from the following sections.

In the course of this paper we proceed first by defining our data sample (§ II). We then investigate the morphology of limb flares (§§ III, IV), and subsequently (§ V) we relate the observed spatial structure (size and height) with the other physical parameters of the region (temperature, density, characteristic times, energy density) in order to determine how these physical characteristics relate to the geometrical configuration of the region. In so doing we conclude (§ VI) that two physically distinct classes of flares do exist that differ both in their morphology and in the physical properties which characterize the emitting regions. The significance of this subdivision into classes will be discussed in the framework of a model which assumes a flare energy-release process operating at coronal heights in a loop configuration; a possible interpretation of the differences observed between the two classes of flares will be proposed.

II. DATA-SELECTION CRITERIA

The data used in this paper were obtained by the American Science and Engineering (AS&E) S-054 experiment on board *Skylab*. The instrument is a grazing incidence X-ray telescope (Vaiana *et al.* 1977) which records images of the Sun on film in sequences of exposures increasing by a factor of 4 from 1/64 s up to a maximum of 256 s. The on-axis spatial resolution is of the order of $2''$. A broad-band spectral resolution in the range 2–60 Å is obtained by inserting six different filters in the optical path. Table 1 gives the nominal passbands of the different filters (between the 0.5% transmission points), including the effects of the reflectivity of the mirrors, the magazine window, and the prefilter. For the purpose of comparing images taken with various filters and exposure times, we refer the reader to the relative response of the different filters at 10^7 K. This quantity is given in Table 1, setting the response of filter 3 equal to 1 (see Vaiana *et al.* 1977 for details). Monochromatic images of bright and small features can also be obtained by inserting a transmission grating into the optical path.

TABLE 1*

Skylab S-054 Experiment Filter Characteristics

Filter	Material	Nominal Passband (Å)	Relative Response at 10^7 K
1.....	Beryllium	2–17	0.30
2.....	Teflon	2–14; 19–22	0.18
3.....	Blank	2–32; 44–54	1.00
4.....	Parylene-N	2–18; 44–57	0.32
5.....	Beryllium	2–11	0.09
6.....	Beryllium	2–14	0.14

* The relative response of different filters is defined in terms of the energy deposited on the film from a solar source at temperature T. For a more detailed discussion, see Vaiana *et al.* (1977).

A scintillation counter and pulse-height analyzer (PHA) with a nominal response to photon energies greater than 10 keV from the whole solar disk are also included in the experiment.

A catalog of flarelike brightenings recorded on the film during the entire *Skylab* mission has been compiled by Kahler and Buratti (1975). In the list flares which have either a temporal profile given by the *Solrad 9* satellite in the spectral bands 1–8 Å and 8–20 Å or a PHA profile have been included. This catalog is the primary source from which the limb flares discussed in this paper have been selected for the purpose of detailed analysis.

The selection criteria used are the following:

1. The flare must be evident in the *Solrad* or S-054 scintillation counter recordings. When two flares occurred simultaneously on the Sun, one on the disk and the other at the limb, the limb flare is included in the morphological analysis; however, the full-disk temporal profile cannot in these cases be used to describe the temporal development of the limb flare or to derive physical parameters.

2. An event is considered to be a limb flare when its heliographic longitude is greater than or equal to 70°. When an Hα flare is reported simultaneously with the X-ray event, the position is assumed to be that of the optical event as given by *Solar Geophysical Data* (1973–1974). If no optical event is reported, the position is estimated by identifying from the X-ray photos the McMath plage region in which the flare occurred and assuming the average coordinates of the region on that day.

3. Only those events are included for which at least one exposure sufficient for the determination of the spatial configuration of the region was taken. Images obtained during any of the flares have been compared with images taken before and after the event. Only those events are included for which the brightenings observed could be unambiguously attributed to the occurrence of a flare.

These criteria gave a total of 43 limb events suitable for analysis. The characteristics of these events are reported in Table 2. For each flare Table 2 gives: (1) date of occurrence; (2) *Solrad 9* temporal profile (time of start, maximum, and end) as reported by *Solar Geophysical Data*; (3) *Solrad* importance (in the system where $Cn = n \times 10^{-3}$, $Mn = n \times 10^{-2}$, $Xn = n \times 10^{-1}$ ergs cm^2 s^{-1} in the spectral band 1–8 Å); (4) associated Hα event, if any (time of start, maximum, and end) as reported by *Solar Geophysical Data*; (5) importance of the optical event; (6) McMath plage region number; (7) heliographic position; (8) time interval in which X-ray photographs were taken by the S-054 telescope during the flare development; and (9) a brief comment on flare morphology.

Our analysis of the data will be based on all the available images, irrespective of the filter used. As discussed by Kahler, Krieger, and Vaiana (1975), the relative brightness of a feature will in general vary from one filter to the other, depending on the temperature of the structure, but the different morphological features will still be present in all filters with approximately the same shape. Similarly, the general characteristics of limb flares will be discussed by considering events observed irrespective of the phase of the flare. As can be seen from Table 2 by comparing *Solrad* profiles with the times in which S-054 observations were made, only a fraction of the events have been observed for their entire duration; most of the observations are limited to the rise or decay phases. We believe that this will not affect the morphological picture of flares that emerges from our data; we postpone a discussion of this point to a later section.

The descriptive analysis of limb flare images will proceed in two steps. In the next section we discuss the general characteristics which result from an overall view of the data. In § IV we describe in detail a small number of events, both for exemplification and for the purpose of investigating the temporal evolution of limb flares in detail.

III. GENERAL CHARACTERISTICS

As previously found for X-ray flares which occur on the disk (Kahler, Krieger, and Vaiana 1975), each limb event appears different from all the others; it is difficult—we have found it impossible—to present a schematic picture of limb flares which can be considered as representative of the *entire* data sample.

However, we have attempted to organize limb flares into different groups by concentrating our attention only on the gross features of the region and its general characteristics. Three principal groupings are introduced: (A) flares characterized by compact loops; (B) flares with a pointlike appearance; and (C) flares characterized by large and diffuse systems of loops.

It is not our intention at this stage to attribute any particular physical meaning to this morphological subdivision; whether or not the different morphologies depend on distinct physical mechanisms or parameters will be investigated in a subsequent section.

Figure 1 (Plate 2) shows examples of events of the first group. (Another example is shown in Fig. 5.) In each case one or more compact and low-lying loops are the main structural features. About 45% of the events studied fall in this group; the identification is more difficult for an additional ~10%. Lengths of the loops range from ~15″ up to ~1′. The maximum observed vertical extent for events in this group is ~25,000 km (December 4 at 1355 UT), but most events show much lower loops; the average is less than ~10,000 km.

Figure 2 (Plate 3) gives examples of the second group of events, which we have termed pointlike events. In these the flare is characterized by the brightening of a very small feature, mostly of the order of 10″ or less, approximately circular in shape. About 30% of the events of our sample can be assigned to this group. In some instances an inspection of a first-generation copy of the original film allowed us to resolve a small loop, but in no case is the possible loop as well defined as in the previous group, and the determination of the geometrical parameters therefore becomes questionable. These pointlike flares appear to be low-lying;

TABLE 2

CHARACTERISTICS OF SELECTED S-054 LIMB EVENTS

DATE (1973-74)	SOLRAD EVENT Start	Peak	End	Import.	Hα EVENT Start	Peak	End	Import.	MCMATH REGION	POSITION	S-054 OBS. Start	End	FLARE MORPHOLOGY
Jun 10	<0900	0921	1400	C2	<0857	0857 0950	>1005	1B	389	N10E90	0807	1254	High loop and subsequently a low-lying point-like feature (1)
Jun 14	0040	0055	0125	<C1	<0047	-	0058	-F	375	N13W70	0031	0124	Compact loop
Jun 14	1810	1817	>1830	<C1	-	-	-	-	375	N13W74	1805	1915	Compact loop
Jun 14	2355	2400	0020	<C1	-	-	-	-	375	N13W80	2351	0018	Compact loop
Jun 29	1940	1953	2300	C5	1947	1949	2007	-B	417	N13E82	2045	2059	High loops
Aug 29	1832	>1840	<1900	>C1	1835 <1843	1836 1844	1842 1851	-F -N	507	S17E72 S14E74	1836	1907	Compact loop
Aug 31	1925	1932	2010	C3	1929	1931	1940	-N	510	N14E79	1916	1940	Compact loop
Sep 5	-	-	-	-	-	-	-	-	501	N15W80	2031	2051	Point-like feature and subsequently a compact loop (2)
Sep 6	0045	0050	0100	C2	-	-	-	-	501	N14W88	0041	0114	Point-like flare or compact loop
Sep 6	-	-	-	-	-	-	-	-	511	N06W(>90)	1217	1222	Compact loop (2)
Sep 6	1445	1457	>1510	C4.7	-	-	-	-	511	N06W(>90)	1442	1520	Point-like feature and subsequently compact loop
Sep 6	1955	2002	>2005	C2.3	-	-	-	-	511	N06W(>90)	1952	2005	Compact loop and a point-like feature at one end of the loop
Sep 9	<1705	1709	1730	C1.6	-	-	-	-	508	N23W82	1711	1719	Compact loop and an adjacent point-like feature
Sep 11	1730	1930	>2400	C5	-	-	-	-	508	N23W(>90)	2201	2210	High loops
Sep 12	0120	0123	0135	C1	-	-	-	-	520	S10W72	0116	0134	Point-like flare
Sep 13	0200	0210	>0220	<C1	-	-	-	-	513	S13W70	0159	0225	Two or more low-lying compact loops
Sep 13	-	-	-	-	-	-	-	-	520	S10W90	1147	1207	Point-like flare (3)
Sep 13	1600	1604	1620	<C1	-	-	-	-	520	S10W90	1556	1605	Point-like flare
Sep 20	-	-	-	-	-	-	-	-	535	N13E80	0958	1025	Point-like flare (4)
Sep 25	>0010	0120	0400	C2	0034	0053	>0132	1N	541	N29E73	0201	0213	High loops (5)
Sep 25	2213	2221	2250	<C1	-	-	-	-	540	S13E80	2211	2223	Point-like flare or small blob
Oct 9	<0113	0115	0140	<C1	-	-	-	-	543	N13W82	0123	0135	Point-like flare
Oct 17	-	-	-	-	-	-	-	-	556	N12W70	1104	1116	Linear structure, maybe a loop (2)
Nov 3	0010	0025	0800	X1.7	0012	0034	0101	2N	584	S18W85	0254	0311	High loops
Nov 13	0025	-	-	<C1	-	-	-	-	618	N14E73	0046	0052	Compact loop
Dec 3	0200	0209	0215	C2	0204	0207	0216	-B	628	S15W71	0200	0237	Two closely spaced point-like features
Dec 3	0535	0552	>0600	<C1	-	-	-	-	628	S10W75	0534	0540	Point-like flare
Dec 4	0850	0855	0910	C9	<0850	0852	>0900	-N	628	S14W87	0903	0908	Point-like flare or small blob
Dec 4	1200	1210	1230	M1.3	1142	1206	1222	1B	628	S13W90	1208	1213	Point-like flare and a faint loop departing from it.
Dec 4	1342	1355	1410	<C1	-	-	-	-	628	S10W88	1345	1418	Compact loop
Dec 5	-	-	-	-	-	-	-	-	628	S10W(>90)	0402	0416	Point-like flare (6)
Dec 5	0508	-	0615	>C1	-	-	-	-	628	S10W(>90)	0537	0554	Compact loop (7)
Dec 16	1320	1330	1350	<C1	1316	1317	1338	--N	664	S17E80	1310	1344	Point-like feature or small loop
Dec 16	2000	2010 2020	>2040	C2.4	1954	2008	2023	--N	664	S17E74	2003	2103	Compact loop
Dec 16	2140	2152	2230	M1.3	2145	2148	2204	--F	664	S19E77	2250	2315	Compact loop rather diffuse
Dec 17	<0030	0042	>0130	M1.1	0029	0032	0057	1B	664	S17E77	0002	0227	Kernel and diffuse structure (8)
Dec 17	0727	0745	>0800	C3.5	0742	0749	0756	--F	664	S19E72	0752	0805	Compact loop
Jan 11	2010	2018 2028	2040	C1.2	-	-	-	-	702	S14E71	2025	2030	Point-like flare or small loop
Jan 15	1050	1105	1530	M1.2	1050	1057	1119	1N	686	N08W85	1247	1434	High loops
Jan 16	0625	0635	>0710	M1.5	-	-	-	-	686	N07W(>90)	0730	0736	Compact loop
Jan 16	2140	-	>2325	>C1	-	-	-	-	686	N07W(>90)	2258	2300	Diffuse blob maybe formed by diffuse loops (9)
Jan 23	<1925	1948	>2015	<C1	-	-	-	-	708	N07W74	2007	2022	Compact loop rather diffuse
Jan 25	0638	0642	>0643	<C1	-	-	-	-	703	S18W(>90)	0647	0653	Point-like flare

(1) PHA profile gives peaks at ∿ 0950 UT and 1123 UT. (2) Another event occurred simultaneously on the disk. (3) No temporal profile. Approximate peak time ∿ 1200 UT. (4) No temporal profile. Approximate peak time ∿ 1010 UT. (5) Solrad profile probably contaminated by another event on the disk. (6) PHA profile gives start at 0405 UT, peak at 0413 UT, end later than 0430 UT. (7) PHA profile gives peak at 0515 UT. (8) PHA profile gives start at 0029 UT. (9) PHA profile gives peak at 2147 UT.

an average vertical extent of the structure is less than ~6500 km.

A few comments are in order at this point. All flares of our groups A and B share the characteristic of being compact structures; most have sizes of the order of a few tens of arcsec. The morphological distinction between the two groups appears rather loose in the sense that there is a continuity of scales from pointlike events to larger and larger loops. For events with characteristic size of the order of ~10″–15″ it is often difficult to decide whether the region we are observing has a looplike structure or is just a true pointlike region.

Second, we note from Table 2 that it appears that both looplike and pointlike flares can be observed in all phases of flare development. In fact, Figure 1 shows loops observed during the rise and decay phases as well as near the peak. Although pointlike flares are observed more frequently during the rise phase in our sample of data, they are also observed during their decay (cf. October 9 at 0130 UT and January 25 at 0642 UT); also, the event of December 3, 0200–0215 UT, although somewhat peculiar, shows the evolution of a flare which maintained the general character of a small compact feature during all its development. We therefore do not believe that the phase in which a flare is observed is a decisive factor in determining whether it appears as a pointlike or as a looplike flare.

Finally, we wish to caution against an identification of our pointlike flares with X-ray kernels, which are small, pointlike, short-lived features found to be, together with loops, the fundamental structures of soft X-ray flares (Kahler, Krieger, and Vaiana 1975). We have defined pointlike events (group B) as those flares in which the *whole* flaring region appears very compact (mostly smaller than 10″); kernels on the contrary can be substructures of a larger flaring region, at times coexistent with loop features or other kernels. However, if the flaring region is dominated by a single kernel, the event would be considered by us to be pointlike.

Let us now examine the third morphological group of limb events, which is characterized by the presence of high, large, diffuse systems of loops which generally appear brighter at the top. About 15% of our events belong to this group. The heights of the loops range from 35,000 km (November 3 at 0025 UT) up to 75,000 km (June 29 at 1953 UT), with an average height of ~50,000 km. Figure 3 (Plate 4) shows two examples of such events. (Another example is given in Fig. 7 and will be discussed in the next section.) *All these have been observed during the decay of long-enduring* ($\gtrsim 3$ *hours*) *events*. The development of high systems of loops whose tops are brighter than the lower sections has also been found by Kahler (1977) for long-decay X-ray flares. The distinctive property associated with events of our group C appears to be their long lifetime (~several hours). The X-ray peak intensity is, on the other hand, widely variable in all groups; we find events ranging in importance from C2 up to X1.7 in group C, and similarly not only low-intensity flares but also flares of importance greater than M1 are observed both for group A (December 16 at 2152 UT and January 16 at 0635 UT) and group B (December 4 at 1210 UT).

In analyzing limb flares observed by the S-056 experiment on *Skylab*, Gibson (1976) stated that about one-half of the events which contain loops presented either a triangular or cusplike shape or a spike structure reminiscent of a helmet streamer. In our data we found a weak indication of such a configuration only in the September 6 (at 1220 UT) event, published by Vorpahl *et al.* (1975) and Gibson (1976). We found no evidence for this in any of the other events. In the September 6 event, however, the flare occurred at the base of an active region (McMath 511) in a zone where the bright core of the active region presented both *before* and *after* the flare an extended spikelike shape (see, for instance, in Fig. 6, the image at 1443:34 UT, taken about two hours later and soon before another flare which occurred at the same position as the event at ~1220 UT). It is our opinion that the apparent spikelike configuration of the flare on September 6 is probably due to an effect of integration along the line of sight of the flare loop and the preexisting bright core of the active region. In general, our conclusion is that no cusplike or spikelike configuration due to the presence of a similar magnetic structure exists in flares.

The distribution of brightness along the structure, which is particularly observable in limb flares, is expected to provide indications about the site of the primary energy deposition and/or the processes of energy and mass transfer. Except for flares of group C, in no case have we observed enhanced brightening at the top of a loop, nor have we observed (within the temporal resolution available to us) the brightening of a small section of a loop followed by the brightening of the entire structure. We observe instead pointlike features or looplike structures which are everywhere bright. The brightening along a loop, however, is often nonuniform; on several occasions we observe that one leg of a loop is brighter than the other (as in the event of December 4 at 1355 UT), or a small brighter knot at one end of a bright larger loop structure (for instance, in the events of September 6 at 2002 UT and on December 5 at 0530 UT). The entire coronal portion of compact structures therefore appears bright during flaring periods, with a tendency to present brighter features (which may either be physically associated with the main structure or just seem associated with it by integration along the line of sight) closer to the foot points than to the top of loops. The long-enduring events of our group C appear to follow a different pattern; the high systems of loops we observe during their decay are generally brighter at their top, these sections sometimes being the only bright parts (see, for instance, Fig. 7).

The capability of our instrument in observing both bright and faint features by taking sequences of photographs with different exposure times allows the localization of the flaring source inside the active region. This allows the determination of the height of

soft X-ray flares with an accuracy previously unattainable. We recall that, before *Skylab*, the determination of the height of X-ray flares was based essentially on indirect methods, either by observing behind the limb events (Kane and Donnelly 1971; McKenzie 1975; Roy and Datlowe 1975), or by observing the same burst with two different spacecraft widely spaced in heliographic longitude (Catalano and Van Allen 1973). As a general rule, we find that, while active-region loops often extend to high altitude (up to 100,000 km and more), the flare brightenings during events of groups A and B always occur at much lower levels, close to the base of active regions. Figure 4 (Plate 5) shows two examples of flares compared with the active region as observed in the preflare and postflare phases. In each case the flare occurred in a small localized zone at a low altitude with respect to the overall structure of the active region. For instance, in the event on January 11, the flaring source appears located at very low height (<6500 km) close to one foot point of a high system ($\sim 75{,}000$ km high) of active-region loops. (Note that the image at 2025:38 UT during the flare was taken in the grating mode.) The loop systems observed during events of group C are instead comparable in height and structure with the high loops typical of the more extended portion of active regions.

IV. DISCUSSION OF INDIVIDUAL EVENTS

In order to provide photographic support for the general properties we have outlined in the previous sections, we shall now describe in more detail a few selected events. This will also give us an opportunity to present some cases which depart in one way or another from the necessarily oversimplified picture presented above.

August 29 (1840 UT): An example of a compact flare loop.—This is a clear example of a flare which occurred in a well-defined loop structure not visible in the preflare and postflare images. Figure 5 (Plate 6) shows the flare loop (at 1836:26 UT and at 1842:26 UT) and for comparison the preflare and postflare appearance of the region (at 1746:12 UT and 1904:06 UT, respectively). The loop is $\sim 15{,}000$ km high with foot points $\sim 30{,}000$ km apart. The brightest part of the loop is located at its southern foot point. As it appears from the northern leg of the loop, the structure is probably formed by two very close loops. This spatial configuration suggests the possibility of formation of neutral sheets and reconnection between two parallel magnetic flux strands, as in the model by Gold and Hoyle (1960) and Piddington (1974). However, this type of configuration, with two closely spaced strands, is not common in our observations and cannot therefore represent a general mechanism for flare occurrence.

September 8 (1457 UT): The development of a compact flare.—As an example of a flare observed for its entire life, we have chosen this event, which occurred in McMath region 511, the same region in which the "spikelike" flare discussed in the previous section (September 6 at 1220 UT) occurred. Figure 6 (Plate 7) shows the temporal development of the event from the preflare to the postflare phase. The structure of the active region shows two main components with two distinct bright cores; the flare appears to occur at the base of a spikelike core with the brightening of a small loop or knot ($<10''$ in size) which evolves into a larger ($\sim 15''$) unstructured region and subsequently into a larger loop. This event occurred behind the limb, and it is likely that we are observing only the upper section of the emitting structure. The event can be interpreted as a small-scale version of flares whose evolution is represented by the successive formation of different systems of loops at increasing heights as found in disk events (Pallavicini *et al.* 1975).

September 11 (1930 UT): A typical example of a flare with large and diffuse systems of loops.—Figure 7 (Plate 8) shows an example of a long-enduring ($\geqslant 6$ hours) event with the brightening of the top of high systems of loops. The comparison between the image at 1630:43 UT (preflare) with the image at 2208:22 UT (taken during the decay phase of the flare) shows that the brightest parts during the flare decay are the upper sections of several high loops already present but fainter in the preflare phase. The bright region at the top of the loops extends horizontally as much as $\sim 85{,}000$ km and appears high over the limb as much as $\sim 50{,}000$ km.

June 10 (0921 UT). A complex X-ray event.—McMath region 389 was the most active region on the Sun during the first *Skylab* mission. The short-term temporal variations which occurred in this region during its passage on the disk have been discussed by Vaiana *et al.* (1973). On June 10 the region was on the east limb and produced a long-enduring and complex X-ray event which lasted for more than 5 hours. Figure 8 (Plate 9) shows a sequence of images taken during that period. The active region at 0808 UT (during the late decay of a previous event) shows the presence of a low-lying bright core with two systems of high loops on both sides. These extended active-region loops range in height from 40,000 to 90,000 km. At ~ 0944 UT we observe an additional loop brighter than the preexisting active-region loops. The brightening of this new loop is the principal cause of the increase of the *Solrad* X-ray flux and appears characteristic of the group of long-enduring events (group C).

At ~ 1135 UT we observe the brightening of the southern of the two pointlike features which formed the bright core of the active region. The southern active-region high loop also appears enhanced. The temporal profile given by *Solrad* results, therefore, from more than one X-ray event. The event also appears complex in Hα, with two reported Hα flares with maxima at 0857 and 0950 UT, respectively. The S-054 scintillation detector gives peaks at 0947 UT, at 0952 UT, and at 1123 UT. A preliminary description of the complex phenomena associated with this event was given previously by Vaiana *et al.* (1974).

A major coronal transient was observed between 0929 and 1001 UT by the HAO white-light coronagraph aboard *Skylab* (MacQueen *et al.* 1974; Hildner *et al.* 1975). The event was preceded by the eruption of

TABLE 3

PHYSICAL PARAMETERS OF SELECTED LIMB EVENTS

EVENT	H (Km)	V (cm^3)	T (^oK)	$\int n^2 dV$ (cm^{-3})	n (cm^{-3})	3nkT (erg cm^{-3})	τ_R (min)	τ_D (min)	τ_T (min)	white-light transient	morph. group
Jun 10(09 21 UT)	45000	6.6×10^{27}	7.7×10^{6}	3.1×10^{48}	2.2×10^{10}	71	30	50	>300	yes	C
Jun 14(00 55 UT)	6000	4.0×10^{26}	10.8×10^{6}	4.6×10^{47}	3.4×10^{10}	150	7	17	45	no	A
Jun 14(18 17 UT)	6000	1.6×10^{27}	6.6×10^{6}	6.2×10^{47}	2.0×10^{10}	55	5	5	>20	no	A
Jun 14(24 00 UT)	6000	4.0×10^{26}	9.9×10^{6}	4.8×10^{47}	3.5×10^{10}	150	3	8	25	no	A
Jun 29(19 53 UT)	75000	1.6×10^{29}	11.0×10^{6}	3.6×10^{49}	1.5×10^{10}	69	4	12	200	yes(?)	C
Aug 29(18 40 UT)	15000	1.0×10^{27}	-	-	-	-	-	-	<28	no	A
Aug 31(19 32 UT)	5000	6.1×10^{26}	9.5×10^{6}	2.7×10^{48}	6.6×10^{10}	260	2	4	45	no	A
Sep 5 (20 45 UT)	5000	$<1.4\times10^{26}$	-	-	-	-	-	-	-	no	A or B
Sep 6 (00 50 UT)	5000	1.4×10^{26}	9.1×10^{6}	1.3×10^{48}	9.6×10^{10}	370	2	4	15	no	A or B
Sep 6 (12 20 UT)	8000	4.6×10^{26}	-	-	-	-	-	-	-	no	A
Sep 6 (14 47 UT)	8000	4.6×10^{26}	9.5×10^{6}	4.6×10^{48}	1.0×10^{11}	400	8	12	>25	no	A or B
Sep 6 (20 02 UT)	6000	9.1×10^{26}	11.1×10^{6}	9.3×10^{47}	3.2×10^{10}	150	2	3	>10	no	A
Sep 9 (17 09 UT)	6000	9.1×10^{26}	9.7×10^{6}	1.3×10^{48}	3.8×10^{10}	150	-	12	>25	no	A
Sep 11(19 30 UT)	50000	1.4×10^{29}	8.3×10^{6}	7.1×10^{48}	7.1×10^{9}	25	60	120	>390	yes	C
Sep 12(01 23 UT)	7000	3.8×10^{26}	9.2×10^{6}	3.1×10^{47}	2.9×10^{10}	110	1	2	15	no	B
Sep 13(02 10 UT)	6000	2.4×10^{27}	12.0×10^{6}	4.2×10^{47}	1.3×10^{10}	65	5	7	>20	no	A
Sep 13(12 00 UT)	<7000	$<3.8\times10^{26}$	-	-	-	-	-	-	-	no	B
Sep 13(16 04 UT)	<7000	3.8×10^{26}	9.6×10^{6}	3.0×10^{47}	2.8×10^{10}	110	4	6	20	no	B
Sep 20(10 10 UT)	<7000	$<3.8\times10^{26}$	-	-	-	-	-	-	-	no	B
Sep 25(01 20 UT)	70000	6.2×10^{28}	7.7×10^{6}	3.1×10^{48}	7.1×10^{9}	23	30	70	>230	yes	C
Sep 25(22 21 UT)	7000	3.8×10^{26}	7.9×10^{6}	5.4×10^{47}	3.8×10^{10}	130	3	9	37	no	B
Oct 9 (01 15 UT)	<7000	$<3.8\times10^{26}$	-	-	-	-	-	-	-	no	B
Oct 17(11 00 UT)	10000	1.5×10^{27}	-	-	-	-	-	-	-	no	A
Nov 3 (00 25 UT)	35000	2.7×10^{28}	11.0×10^{6}	1.2×10^{50}	6.5×10^{10}	300	13	50	470	yes	C
Nov 13(01 00 UT)	12000	2.8×10^{27}	-	-	-	-	-	-	-	no	A
Dec 3 (02 09 UT)	7000	3.8×10^{26}	10.1×10^{6}	1.7×10^{48}	6.7×10^{10}	280	2	2	15	no	B
Dec 3 (05 52 UT)	5000	$<1.4\times10^{26}$	7.3×10^{6}	1.1×10^{48}	8.9×10^{10}	270	4	4	>25	no	B
Dec 4 (08 55 UT)	8500	6.6×10^{26}	9.0×10^{6}	1.1×10^{49}	1.3×10^{11}	490	4	5	20	no	B
Dec 4 (12 10 UT)	6000	$<2.7\times10^{26}$	10.7×10^{6}	9.7×10^{48}	1.9×10^{11}	720	4	7	30	no	B
Dec 4 (13 55 UT)	25000	2.4×10^{27}	-	-	-	-	7	8	28	no	A
Dec 5 (04 13 UT)	7000	$<3.8\times10^{26}$	-	-	-	-	-	-	-	no	B
Dec 5 (05 30 UT)	18000	5.0×10^{27}	-	-	-	-	-	-	-	no	A
Dec 16(13 30 UT)	6000	2.7×10^{26}	7.3×10^{6}	1.2×10^{48}	6.7×10^{10}	200	10	13	30	no	A or B
Dec 16(20 20 UT)	4000	2.7×10^{26}	9.2×10^{6}	2.6×10^{48}	9.8×10^{10}	380	6	8	>40	no	A
Dec 16(21 52 UT)	9000	7.4×10^{26}	10.1×10^{6}	1.2×10^{49}	1.3×10^{11}	550	5	10	50	no	A
Dec 17(00 42 UT)	7000	2.1×10^{27}	9.3×10^{6}	1.2×10^{49}	7.6×10^{10}	300	2	6	>60	no	B
Dec 17(07 45 UT)	6000	2.5×10^{27}	8.2×10^{6}	5.2×10^{48}	4.6×10^{10}	160	6	7	>33	no	A
Jan 11(20 25 UT)	<6000	$<2.7\times10^{26}$	8.5×10^{6}	1.5×10^{48}	7.4×10^{10}	260	3	3	30	no	A or B
Jan 15(11 05 UT)	40000	1.35×10^{29}	8.0×10^{6}	2.0×10^{49}	1.2×10^{10}	40	10	45	280	yes	C
Jan 16(06 35 UT)	12000	8.1×10^{26}	9.3×10^{6}	1.7×10^{49}	1.4×10^{11}	550	5	7	>45	yes	A
Jan 16(22 00 UT)	15000	7.2×10^{27}	-	-	-	-	-	-	>85	no	A
Jan 23(19 48 UT)	10000	2.2×10^{27}	6.5×10^{6}	2.2×10^{48}	3.2×10^{10}	87	12	20	>50	no	A
Jan 25(06 42 UT)	7000	$<3.8\times10^{26}$	8.4×10^{6}	1.1×10^{48}	5.4×10^{10}	190	2	-	>5	yes(?)	B

a prominence at 0815 UT. The prominence was observed by ground-based telescopes to ascend to 0.4 $R_\odot$. At 0930 UT a bright surge was observed out to 0.2 $R_\odot$. As we shall see in the following sections, the association with white-light coronal transients and active prominences provides an important clue for understanding the physics of a class of limb flares.

V. PHYSICAL PARAMETERS

The subdivision into three groups that we have introduced above is based solely on general morphological characteristics. In order to investigate whether there is a physical significance in this subdivision, we have determined the plasma parameters of the region by combining full-disk data obtained by *Solrad* with our spatially resolved observations. In this way we have obtained values of height, volume, temperature, emission measure, density, and characteristic times, and have correlated these quantities, seeking a physically more meaningful classification which might be related to the morphological appearance of limb flares.

The geometrical parameters (height and size) can be measured on the photographs. An accurate determination of size is typically done by microdensitometry of photographs and by taking the scattering effect of the telescope into account. This procedure is rather long and too detailed for the purpose of analyzing a large sample of data where one is looking for only gross characteristics. Therefore we have limited ourselves to estimating the size by a direct measure of the photographic images. For regions larger than $\sim 15''$ the effect of scattering by the telescope mirror can be estimated to be of the order of $\sim 20\%$; it is somewhat larger for smaller regions (Pallavicini *et al.* 1975; Kahler, Petrasso, and Kane 1976). The height of the structures and the estimated volumes are reported in columns (2) and (3) of Table 3.

Temperatures and volume emission measures $\int_V n^2 dV$ at the peak of the events have been evaluated by the ratio of *Solrad 9* fluxes in the spectral bands 1–8 Å and 8–20 Å. The procedure has been described by Dere, Horan, and Kreplin (1974) and is based on the continuum free-free and free-bound spectrum of Culhane (1969), the line spectrum of Tucker and Koren (1971), and experimental values of detector efficiencies. Temperatures and emission measures are given in columns (4) and (5) of Table 3.

From the emission measure $\int_V n^2 dV$ given by *Solrad* and the volume estimated from the X-ray images, the average density of the region can be deduced. The values of density are only lower limits, both because our estimate of the volume, not corrected for scattering, is an upper limit, and because the spectral responses of *Solrad* detectors and of S-054 filters are somewhat different (see Kahler, Petrasso, and Kane 1976 for details). Column (6) in Table 3 gives the density, while in column (7) we have reported the energy density $3nkT$, k being the Boltzmann constant.

The rise time τ_R and the decay time τ_D at $1/e$ of the peak intensity value and the total duration τ_T of the events (above the background level) are deduced from the *Solrad* temporal profiles in the spectral bands 1–8 Å. These three characteristic times are reported in columns (8), (9), and (10) of Table 3.

We have also looked for an association of our limb events with white-light coronal transients. In column (11) of Table 3 we have reported whether or not a coronal transient was observed by the HAO white-light coronagraph on board *Skylab* (MacQueen 1975) at the same time and at the same position angle as the X-ray flare.

The estimated parameters reported in Table 3 allow a statistical comparison to be made between different events. We shall investigate the relationship between the various parameters by means of plots in which the

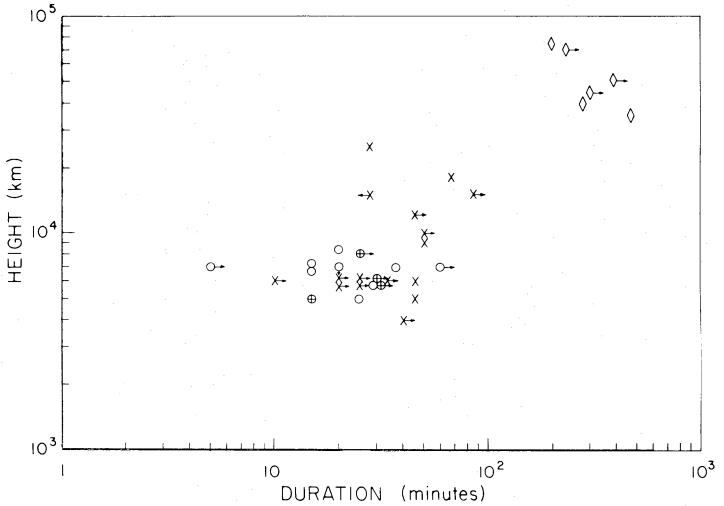

FIG. 9.—Plot of the height (km) of X-ray limb flares versus the total duration (minutes). Different symbols are used for the three morphological groups discussed in the text. *Crosses*, flares with compact loops (group A); *circles*, pointlike flares (group B); *diamonds*, flares with large and diffuse systems of loops (group C). Circles enclosing crosses are used for the cases in which the attribution of the event to group A or group B is uncertain.

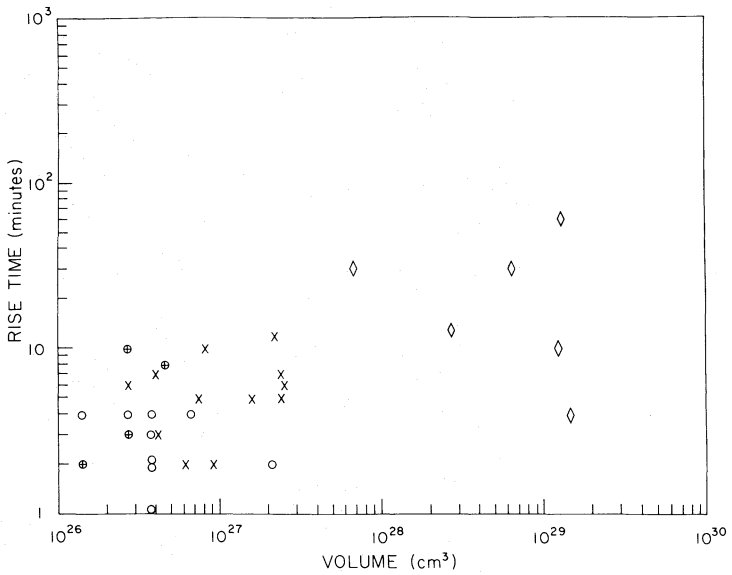

FIG. 10.—Plot of the rise time (minutes) of X-ray limb flares versus the volume (cm^3). Symbols have the same meaning as in Fig. 9.

experimental points are distinguished according to the morphological subdivision of limb flares in different groups. The group to which we have attributed each of the events is reported in the last column of Table 3.

The temperatures we obtain are around 10^7 K (ranging from 6.5×10^6 up to 12×10^6 K) and the densities are of the order of $\sim 5 \times 10^{10}$ cm^{-3} (ranging from 7×10^9 up to 1.9×10^{11} cm^{-3}). The emission measure ranges from 3.0×10^{47} up to 1.2×10^{50} cm^{-3}. These values are typical for X-ray flares in this spectral region (Hudson 1975).

In Figure 9 we have plotted the height of flare structures versus the total duration of the events (as measured by the *Solrad* flux above the background level). The experimental points group into two separate regions. Compact loops (*crosses*) and pointlike events (*circles*) appear to group together, while events with large and diffuse systems of loops (*diamonds*) are all of longer duration ($\gtrsim 3$ hours) and greater height. The plot suggests the existence of two distinct classes of flares, one consisting of both our morphological groups A and B, the other of only the long-enduring events in group C. No systematic difference appears to be present between flares with compact loops and pointlike events.

Figures 10 and 11 give the rise time and decay time, respectively, of the different events as a function of the volume. Again it appears that, statistically, flares of group C, with their longer rise time and particularly their longer decay times (with the exception of the event on June 29 at 1953 UT), and with their larger volume, tend to behave differently from flares of both groups A and B.

The separation of the three morphological groups in only two physically distinct classes appears also in a plot of the energy density $3nkT$ versus the height (Fig. 12). There is a general tendency of events of group C to have a lower energy density than events of groups A and B. There are also, however, some exceptions, particularly the event on November 3 at 0025 UT, which has an energy density of 300 ergs cm^{-3} despite its morphological appearance as an event with large and diffuse systems of loops. The event on November 3 was also the most intense (*Solrad* importance X1.7) of the flares we have examined. It is not surprising that a correlation may exist between the peak flux of an event and its energy density. In Figure 13 we have plotted the energy density $3nkT$ versus the peak flux measured by the *Solrad* satellite in the spectral band 1–8 Å with the preflare value subtracted. While the events of group C appear to have systematically lower energy density than events of groups A and B of comparable peak flux, there is a tendency for all events to have higher energy density for increasing values of the peak flux.

Finally, we note from Table 3 that flares with large and diffuse systems of loops (group C) are associated with a white-light coronal transient (only for the event on June 29 at 1953 UT is the association somewhat dubious), while for flares of groups A and B, a white-light coronal transient is never observed except for the January 16 (at 0635 UT) event (and possibly the January 25 at 0642 UT event).

The evidence presented in Figures 8–13 and the correlation of only events of group C with white-light coronal transients indicate the existence of two classes of flares which correspond to different physical characteristics of the emitting region. Class I comprises compact flares (both pointlike events and compact-loop events) with smaller volume and lower height, faster rise and decay times, and shorter duration. They are not associated with white-light coronal transients, and they have higher energy density. Class II is constituted by the events with large, high,

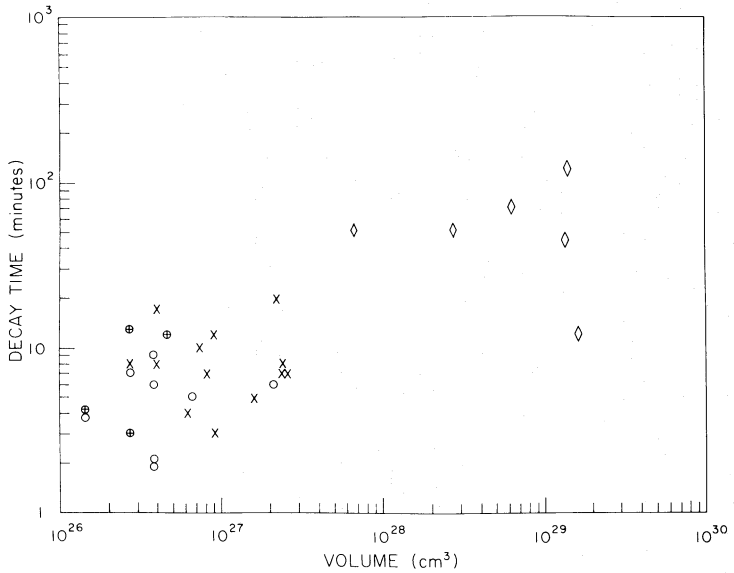

FIG. 11.—Plot of the decay time (minutes) of X-ray limb flares versus the volume (cm^3). Symbols have the same meaning as in Fig. 9.

diffuse systems of loops. They are long-enduring events, with longer rise and decay times and larger volume. They have lower energy density and are associated with white-light coronal transients. In the next section we shall indicate another important characteristic of flares of class II, their association with prominence eruption or activation.

VI. DISCUSSION

a) Identification of Two Physically Distinct Classes of Flares

The principal result of our analysis of limb events is, in our opinion, the identification of two physically distinct classes of flares, one comprising compact flares (our morphological groups A and B) and the other only larger and diffuse events (group C). We expect that this result has significant consequences for modeling solar flaring regions.

Between events with compact loops (group A) and those with pointlike flares (group B), no obvious physical difference appears to exist. Flares of these two groups are morphologically different, but, as we have noted above, there is a continuity of scales going from pointlike events to larger and larger loops. The analysis of their physical parameters does not show

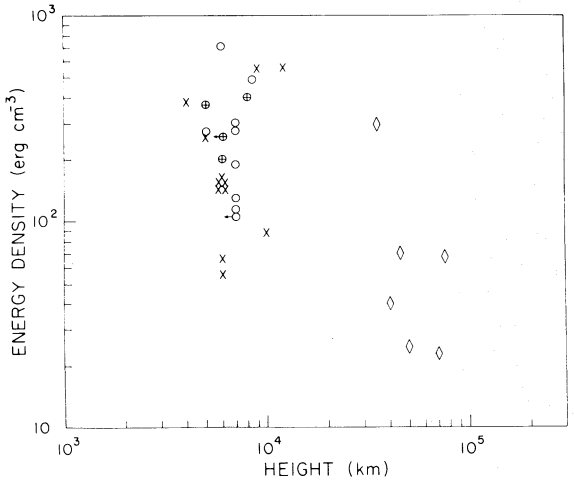

FIG. 12.—Plot of the energy density $3nkT$ (ergs cm^{-3}) of X-ray limb flares versus the height (km). Symbols have the same meaning as in Fig. 9.

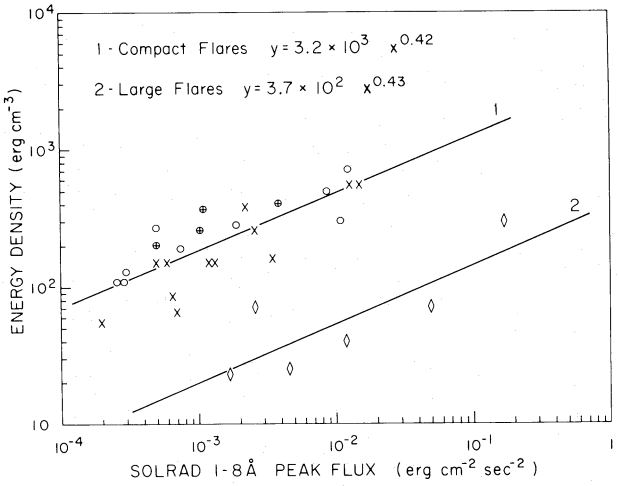

FIG. 13.—Plot of the energy density $3nkT$ (ergs cm^{-3}) of X-ray limb flares versus the peak flux (ergs $cm^{-2}\ s^{-1}$) given by the *Solrad 9* satellite in the spectral band 1–8 Å. Symbols have the same meaning as in Fig. 9. The two straight lines are least-squares fits for events of group C and of group A plus B, respectively.

any systematic difference between the two groups. Moreover, no correlation exists between the morphological appearance of a flare and its peak intensity (as measured by the *Solrad* importance) or the phase in which the event is observed (see Table 2). Our conclusion is that pointlike flares do not constitute a separate class but are probably formed by unresolved loops. The same conclusion was reached for X-ray kernels by Kahler, Petrasso, and Kane (1976), on the basis that no apparent increase of size of kernels was observed over times longer than the characteristic times for heat conduction or mass transfer from a region such as a kernel with pressure higher than the surrounding regions. Gibson (1976) found that $\sim 30\%$ of limb events observed by the S-056 experiment appeared as small knots but did not classify them as a separate class, following the suggestion of Vorpahl *et al.* (1975) that they were unresolved loops close to the resolution of the telescope.

Flares of group C (large and diffuse loops) are, on the contrary, physically different from the other two groups. They have generally longer rise and decay times and longer duration. They are higher than compact flares, and their energy density is on the average almost one order of magnitude less than for compact events. The volume of plasma involved by these events is larger than for flares of groups A and B, and they are the only events which are correlated with white-light coronal transients.

The other major difference which appears to be present between our events of class I and events of class II concerns the distribution of brightness along the structure. While events with large and diffuse loops are consistently brighter at the top, indicating an increase of temperature or density or both at the tops of loops, compact flares are bright along the entire structure with a tendency to be brighter at the foot points. In the compact flare case, however, it is more difficult to decide whether the enhanced brightening at the foot points occurs in a single structure (for instance, owing to an increase of density at the foot points) or is just due to the presence of separated unresolved structures. The additional pointlike features occasionally observed close to the foot points of compact loops may themselves be small unresolved loops. We call attention, for instance, to the event on June 10 (at 0921 UT) in which the small dots which formed the low-lying core of the active region (see Fig. 8) are actually small loops in bipolar magnetic zones, as shown by an analysis of the region during its passage on the disk (Vaiana *et al.* 1973).

b) *Association of Flares of Class II with Active Prominences*

In an analysis of X-ray and UV observations of coronal changes associated with an Hα disappearing filament, Sheeley *et al.* (1975) found a statistical correlation between long-enduring *Solrad* X-ray bursts (and associated gradual rising and falling microwave bursts) and white-light transients in the outer corona. They also found that at least two-thirds of the observed long-enduring events involved either the eruption or major activation of a prominence. Are flares of class II coincident as a group with the events studied by Sheeley *et al.* (1975)? In our sample of data, all long-enduring events with duration greater than ~ 3 hours were accompanied by white-light coronal transients (see Table 3). In all cases an active prominence or prominence eruption was reported (NOAA reports), the only exception being the event of June 29 (at 1953 UT), for which the association with a white-light coronal transient is also somewhat dubious. Flares of class I, on the contrary, did not produce white-light coronal transients except in one or possibly two instances. This is consistent with the results of Munro *et al.* (1974), who found that eruptive prominences produce approximately 3 times the number of white-light coronal transients that flares in general do. An association between eruptive prominences and long-enduring soft X-ray events was early suggested by Kreplin, Chubb, and Friedman (1962). Roy and Tang (1975) studied slow ($\gtrsim 1$ hour) X-ray bursts which presented filament disruptions in Hα. Drake (1971) and Horan (1971), on the other hand, failed to find any difference, apart from the time scale, between long-enduring and short-lived events in regard to the parameters reduced by means of full-disk soft X-ray detectors.

There are a number of optical phenomena that somewhat resemble our events of class II and can provide clues for understanding the physical processes which occur in them. Fast coronal changes observed in the optical lines of Fe XIV at 5303 Å and Ca XV at 5694 Å are occasionally observed in association with flares or some other Hα activity (Dunn 1971; De Mastus, Wagner, and Robinson 1973). As reported by Waldmeier (1974), the densest and hottest condensations of coronal material during fast coronal phenomena typically occur not close to the Sun limb but at a height of $\sim 40{,}000$ km. This height is comparable with the average altitude of the top of the high X-ray loops we observe in flares of class II. Formations of flare-associated loop-prominence systems with height up to $\sim 10{,}000$ km are often observed in Hα (Bruzek 1964, 1969) during the decay and postflare phases of large events. The postflare loops survive for many hours after the optical event and are also observed in the green line at 5303 Å (Bruzek and De Mastus 1970).

Taken together, these observations suggest that flares of our class II represent a family of long-enduring events associated with activation and possible eruption of prominences, characterized by the development of high systems of loops in X-rays (and possibly at UV and optical wavelengths as well), and producing transients in the outer corona. Flares of class II are essentially the same type of phenomena as the events studied by Sheeley *et al.* (1975) and Kahler (1977).

c) *Interpretation of the Two Classes of Flares*

There are several relevant facts which differentiate physically between the two classes of flares we have

identified and which suggest a possible interpretation. In particular, we have seen that flares of class II have on the average longer characteristic times and larger characteristic lengths than flares of class I. Their energy density is on the average lower by almost one order of magnitude than that of compact flares. Further, the distribution of brightness along their structure is different; flares of class II are consistently brighter at the top. These flares produce more pronounced effects in the outer corona (as shown by the occurrence of white-light transients) and in addition are associated with prominences which become active and frequently erupt at the time of flaring.

There is another constraint which applies to flares in general. As shown in Table 3, the densities we observe in flares of both class I and class II (ranging from 7×10^9 to 1.9×10^{11} cm^{-3}) are generally larger by about one order of magnitude than typical active-region loop densities (Davis *et al.* 1975). Moreover, it is well known that the volume emission measure $\int_V n^2 dV$ increases by one or two orders of magnitude during flares (Datlowe, Hudson, and Peterson 1974). Additional material must, therefore, be supplied to the flaring source; this additional material must be cool, since we have found no evidence from X-ray photographs for an accumulation of coronal temperature material prior to the flare. The latter possibility is also excluded by microwave observations of active regions in the preflare stage (Ohki 1975). Hence the excess of mass which appears to be present in the flaring source either must come from outside the corona or, if locally present in the corona prior to the flare, must be there at a temperature sufficiently low so as not to contribute appreciably to microwave and X-ray emission. The physical differences, which we find distinguish the two classes of flares, and the association of class II flares with active prominences, suggest that the two flare classes have different sources of the denser and cooler material; in one case, this material may come from chromospheric levels by means of evaporation (class I), and in the other it is already present at coronal heights in the form of a prominence (class II).

That there is a strict association between prominences and transient phenomena observed in the X-ray corona is also indicated by the existence of another class of X-ray phenomena analyzed by Webb, Krieger, and Rust (1976). They have studied X-ray enhancements observed in association with the disappearance of Hα filaments away from active regions. These large-scale events are generally not associated with chromospheric flares and are too faint to produce a detectable *Solrad* profile above the background level. For the particular event they studied in detail (which is assumed to be typical for this class of events), they found an energy density of ~ 1 ergs cm^{-3}, more than a factor of 10 lower than the average density of our class II flares. Typically the duration of the events associated with filament disappearances away from active regions ranges from ~ 3 hours to ~ 40 hours with a size scale of the order of several arcmin. They are, therefore, events with longer time scales, larger size scales, and lower energy density than the flares belonging to class II. The association between the disappearance of the Hα filament and the enhanced brightness of the X-ray corona close to the filament suggests that the phenomena studied by Webb, Krieger, and Rust (1976) are caused by heating of previously cooler material, possibly coming from the filament itself.

Although all the transient phenomena in the X-ray corona (including our two classes of flares and the events studied by Webb *et al.*) may appear morphologically different, there are some analogies which are suggestive of a possible common relationship. In particular, the monotonic trends of the energy density, size scale, and time scale for transient phenomena in the corona suggest the existence of a continuous range of activity. We proceed from high energy density ($\sim 10^2$–10^3 ergs cm^{-3}), compact, short-lived flares to more diffuse and lower energy density (~ 10–10^2 ergs cm^{-3}) events associated with prominence activations and white-light coronal disturbances, down to the even less energetic (~ 1 ergs cm^{-3}), larger length scale, and longer lifetime events associated with filament disappearances but not with flares.

The data analyzed in this paper do not allow a unique determination of the nature of the basic mechanism responsible for the transient phenomena in the X-ray corona. We suspect (and assume tentatively as a working hypothesis) that the basic mechanism is substantially similar in all these phenomena and that it operates at coronal levels in a loop configuration, and that differences between the various classes of transient phenomena are primarily due to different physical conditions present in the regions prior to the transient event.

This hypothesis leads us to expect that, for compact flares of class I, the energy released in the coronal portion of a loop structure is conducted downward, producing evaporation of chromospheric material and filling of the structure from below, thereby increasing the emission measure. For flares of class II, the distribution of temperature and density in the preexisting active-region loop may be such as to allow condensation of material at the top of the loop in the form of a prominence. Whatever the mechanism of condensation may be, cool chromospheric material is actually observed to be present at coronal levels, and the observed activation of the filament indicates that it plays an important role in the whole flare process. The primary effect of the flare energy release may in this case be the direct heating of cool chromospheric material from the prominence, thereby again increasing the X-ray emission measure.

We have seen that flares of class II have the morphological characteristic of being brighter at the top. This fact indicates, first, that the heating is probably occurring at the top of the loop, where the filament material is located; and second, that the pressure at the top of the loop is substantially higher than in the lower sections. (The possibility of interpreting brightness differences in X-ray images as an indication of pressure differences has been discussed by Kahler [1976].) Such a configuration is not hydrostatically

stable; we have found, however, that this characteristic is observable during the decay phase of all events of class II, irrespective of the particular time of the observation after the flare peak. This observation suggests that the upward pressure gradient along the loop may last for a substantial fraction of the flare lifetime (~hours) and therefore much longer than the characteristic times for heat conduction or mass transport. The only possible explanation of this seems to be that we are actually observing a dynamic phenomenon in which cool material from the filament is continually heated at the top of the loop and falls down along the magnetic lines of force. In any case, the rate of energy input during the long-enduring events of class II must be slow, and a continual input of energy and mass at the top of the loop appears to be required over a considerable fraction of the lifetime of the events.

Our interpretation differs somewhat from that proposed by Kahler (1977) for long-decay events. He also noticed a general relationship between long-decay events and the events analyzed by Webb, Krieger, and Rust (1976) but suggested that at least part of the long-decay events he studied are the X-ray analog of the flare-associated loop prominence systems observed in Hα following strong chromospheric flares (Bruzek 1964). In our view, the high loops observed in X-rays during flares of class II are not simply a secondary process characteristic of the decay phase of the events owing to the propagation of the flare disturbance to higher and higher levels in the corona, but are intrinsically related to a specific physical condition of the region at the time of the flare onset. The relevant fact which determines the physics of this kind of event is, according to our interpretation, the local presence of cool condensed material in the form of a prominence. We note that Kahler (1977) found a tendency for long-decay events to occur preferentially in old active regions. This is consistent with our picture, because flare-associated filaments generally do not appear in young active regions (Švestka 1976); therefore one expects to find a lower rate of occurrence of class II flares in young active regions, since they require cool material from prominences. In addition, it is not surprising that flares like those of class II which are associated with larger loops occur more frequently in old active regions where the magnetic field is decayed and more diffuse.

d) Magnetic Configuration

It appears evident from the observations presented in the previous sections that the magnetic configuration in which the thermal processes responsible for soft X-ray emission take place is a closed one. This does not, however, rule out a flare model such as that by Sturrock (1968, 1972) in which a tearing-mode instability occurs at the boundary between a closed magnetic configuration and an open one. We have seen that we do not find evidence of "helmet-streamer" shapes in our data; however, the plasma region heated after the instability has occurred may assume the form of a closed magnetic loop, as discussed by Strauss and Papagiannis (1971). A similar situation would also occur in Syrovatskii's model (1969), in which a simple bipolar field interacts with a more or less uniform external field. Analogously, other models, such as those by Alfvén and Carlqvist (1967) and Cheng and Spicer (1975), which consider instabilities as occurring in a closed magnetic configuration owing to current interruption or a screw-pinch, are consistent with our data. In a few cases we have observed two closely spaced pointlike features (for instance, in December 3 at 0209 UT) or two adjacent loop structures (August 29 at 1840 UT; see Fig. 5), but these events appear to be too peculiar to be interpreted as evidence of the existence of neutral sheets with possible reconnection.

A more precise determination of the basic magnetic model does not seem possible at this stage. More theoretical work has to be carried out if we are to understand the details of the observations. In particular, questions about the formation of prominences and their location in the overall structure of the region, and about the relationship between prominence activation and flare mechanism, need a more quantitative investigation if we are to understand the physics of the events of class II and their differences with respect to compact flares.

Gibson (1976) and Cheng (1976) interpreted large-scale deformations observed in X-ray and UV images of flares as evidence of a kink instability, indicating the flow of substantial currents in flare loops. We have looked for such an effect in our data. We did not find any conclusive evidence to support this interpretation. It is our impression that changes observed in X-ray images are most probably related to the brightening of different preexisting magnetic configurations, rather than being due to a restructuring of the magnetic field.

VII. SUMMARY

We have examined soft X-ray photographs of 43 solar flares which occurred within 20° from the Sun limb. We have found that:

1. *a*) We can organize limb flares into three main morphological groups: (A) flares characterized by compact loop structures; (B) flares with a pointlike appearance; and (C) flares characterized by large and diffuse systems of loops.
   b) The vertical extent for events of groups A and B is generally small, less than $\sim 10^4$ km for most events. They lie very low in the structure of active regions.
   c) The vertical extent for events of group C is larger, with loops extending up to 50,000 km and more, which are comparable in height and structure with the high loops characteristic of the extended portion of active regions.
   d) Events of group C are generally bright only at their top, while events of groups A and B are bright along their entire structure with a tendency to be brighter in the lower sections of loops or to show additional bright features close to their foot points.

2. *a*) From a comparison of the spatial structure of flares with their physical parameters (height, volume, energy density, characteristic times) together with the correlation with white-light coronal transients and Hα active prominences, there appear to be two physically distinct classes of flares: class I, which combines the morphological groups A and B, and class II, which comprises only events of group C.
   b) Events of class I are compact flares (both pointlike events and compact-loop events) with smaller volume ($\sim 10^{26}$–10^{27} cm^3) and lower height ($\lesssim 10^4$ km), faster rise and decay times, and shorter duration (~tens of minutes). They have higher energy density ($\sim 10^2$–10^3 ergs cm^{-3}) and are not associated with white-light coronal transients.
   c) Events of class II are long-enduring events (~hours), with longer rise and decay times and greater height (~50,000 km). They have larger volume ($\sim 10^{28}$–10^{29} cm^3) and lower energy density (~ 10–10^2 ergs cm^{-3}). They are associated with prominence eruption or activation and with white-light coronal transients.
   d) The absence of any systematic physical difference between events with compact loops and pointlike flares indicates that the latter are most probably small loops not resolved by the telescope.
3. The basic magnetic configuration shown by limb flares is a closed one, in the form of a loop structure. No evidence is found of spikelike or cusplike structures reminiscent of helmet streamers.
4. No large-scale deformation of the flare structure is observed that could be interpreted unambiguously as evidence of restructuring of the magnetic field.

We have interpreted the observed differences between the two classes of flares we have identified as due to a difference in the source from which additional mass is supplied to the flaring region. In particular, we have suggested that compact flares of class I are loops filled from below by evaporated chromospheric material, while flares of class II are probably produced by direct heating of cool condensed material present at coronal heights in the form of a prominence. In this interpretation, the observations have shown that flares of class II require a continuous input of energy and matter at the top of the high loops and a continuous flow of the heated material from the top of the loops to lower levels.

We are indebted to the scientists, engineers, and technical staff of the S-054 team who participated in the design, construction, and operation of the experiment. It is a pleasure to thank R. Rosner and G. Noci for their critical reading of the manuscript and helpful comments. One of the authors (R. P.) also wishes to acknowledge useful discussions with S. Kahler. We thank Mrs. B. Duncan for typing the paper, and R. Haggerty and S. Bichisecchi for helping in the photographic presentation of the data.

This work is part of an ongoing *Skylab* collaboration between the USA and Italy supported by NASA (contracts NAS8-27758 and NAS8-31374) and by Consiglio Nazionale delle Ricerche.

REFERENCES

Alfvén, H., and Carlqvist, P. 1967, *Solar Phys.*, **1**, 220.
Beigman, I. L., Grineva, Yu. I., Mandel'stam, S. L., Vainshtein, L. A., and Zhitnik, I. A. 1969, *Solar Phys.*, **9**, 160.
Bruzek, A. 1964, *Ap. J.*, **140**, 746.
———. 1969, in *Solar Flares and Space Research*, ed. C. de Jager and Z. Švestka (Amsterdam: North-Holland), p. 61.
Bruzek, A., and De Mastus, H. L. 1970, *Solar Phys.*, **12**, 447.
Catalano, C. P., and Van Allen, J. A. 1973, *Ap. J.*, **185**, 335.
Cheng, C. C. 1976, Naval Research Laboratory preprint.
Cheng, C. C., and Spicer, D. S. 1975, in *IAU Symposium No. 68, Solar Gamma-, X-, and EUV Radiation*, ed. S. R. Kane (Dordrecht: Reidel), p. 423.
Cheng, C. C., and Widing, K. G. 1975, *Ap. J.*, **201**, 735.
Culhane, J. L. 1969, *M.N.R.A.S.*, **144**, 375.
Datlowe, D. W., Hudson, H. S., and Peterson, L. E. 1974, *Solar Phys.*, **35**, 193.
Davis, J. M., Gerassimenko, M., Krieger, A. S., and Vaiana, G. S. 1975, *Solar Phys.*, **45**, 393.
De Mastus, H. L., Wagner, W. J., and Robinson, R. D. 1973, *Solar Phys.*, **31**, 449.
Dere, K. P., Horan, D. M., and Kreplin, R. W. 1974, *J. Atm. Terr. Phys.*, **36**, 989.
Drake, J. F. 1971, *Solar Phys.*, **16**, 152.
Dunn, R. B. 1971, in *Physics of the Solar Corona*, ed. C. Macris (Dordrecht: Reidel), p. 114.
Gibson, E. G. 1976, Aerospace Report No. ATR-76(7405)-2.
Gold, T., and Hoyle, F. 1960, *M.N.R.A.S.*, **120**, 7.
Hildner, E., Gosling, J. T., MacQueen, R. M., Munro, R. H., Poland, A. I., and Ross, C. L. 1975, *Solar Phys.*, **42**, 163.
Horan, D. M. 1971, *Solar Phys.*, **21**, 188.
Hudson, H. S. 1975, in *X-rays in Space*, ed. D. Venketesan (Calgary: University of Calgary Press), p. 233.
Kahler, S. W. 1976, *Solar Phys.*, **48**, 255.
———. 1977, preprint ASE-4007.
Kahler, S. W., and Buratti, B. J. 1975, unpublished catalog of flares observed by the S-054 experiment on *Skylab*.
Kahler, S. W., Krieger, A. S., and Vaiana, G. S. 1975, *Ap. J. (Letters)*, **199**, L127.
Kahler, S. W., Petrasso, R. D., and Kane, S. R. 1976, *Solar Phys.*, **50**, 179.
Kane, S. R., and Donnelly, R. F. 1971, *Ap. J.*, **164**, 151.
Kreplin, R. W., Chubb, T. A., and Friedman, H. 1962, *J. Geophys. Res.*, **67**, 2231.
Krieger, A. S., Vaiana, G. S., and Van Speybroeck, L. P. 1971, in *IAU Symposium No. 43, Solar Magnetic Fields*, ed. R. Howard (Dordrecht: Reidel), p. 397.
Kundu, M. R., Alissandrakis, C. E., and Kahler, S. W. 1976, *Solar Phys.*, **50**, 429.
MacQueen, R. M. 1975, unpublished catalog of coronal transients observed by the S-052 experiment on *Skylab*.
MacQueen, R. M., Eddy, J. A., Gosling, J. T., Hildner, E., Munro, R. H., Newkirk, G. A., Jr., Poland, A. I., and Ross, C. L. 1974, *Ap. J. (Letters)*, **187**, L85.
McKenzie, D. L. 1975, *Solar Phys.*, **40**, 183.
Munro, R. H., Gosling, J. T., Hildner, E., MacQueen, R. M., Poland, A. I., and Ross, C. L. 1974, in *Flare-related Magnetic Field Dynamics* (Boulder, CO: High-Altitude Observatory), p. 139.
Neupert, W. M., Thomas, R. J., and Chapman, R. D. 1974, *Solar Phys.*, **34**, 349.
Ohki, K. 1975, *Solar Phys.*, **45**, 435.
Pallavicini, R., and Vaiana, G. S. 1976, *Solar Phys.*, **49**, 297.
Pallavicini, R., Vaiana, G. S., Kahler, A. S., and Krieger, A. S. 1975, *Solar Phys.*, **45**, 411.

Petrasso, R. D., Kahler, S. W., Krieger, A. S., Silk, J. K., and Vaiana, G. S. 1975, *Ap. J. (Letters)*, **199**, L127.
Piddington, J. H. 1974, *Solar Phys.*, **38**, 465.
Roy, J. R., and Datlowe, D. M. 1975, *Solar Phys.*, **40**, 165.
Roy, J. R., and Tang, F. 1975, *Solar Phys.*, **42**, 425.
Sheeley, N. R., Jr., Bohlin, J. D., Brueckner, G. E., Purcell, J. D., Scherrer, V. E., Tousey, R., Smith, J. B., Speich, D. M., Tandberg-Hanssen, E., Wilson, R. M., De Loach, A. C., Hoover, R. B., and McGuire, J. P. 1975, *Solar Phys.*, **45**, 377.
Solar Geophysical Data. 1973–1974, US Department of Commerce, NOAA, Environmental Science Services Administration, Boulder, CO.
Strauss, F. M., and Papagiannis, M. D. 1971, *Ap. J.*, **164**, 389.
Sturrock, P. A. 1968, in *IAU Symposium No. 35, Structure and Development of Solar Active Regions*, ed. K. O. Kiepenheur (Dordrecht: Reidel), p. 471.
———. 1972, in *Solar Activity—Observations and Predictions*, ed. P. S. McIntosh and M. Dryer (Cambridge: MIT Press), p. 173.
Švestka, Z. 1976, *Solar Flares* (Dordrecht: Reidel), p. 216.
Syrovatskii, S. I. 1969, in *Solar Terrestrial Physics/1970*, Part I, ed. E. R. Dyer and C. de Jager (Dordrecht: Reidel), p. 119.
Tucker, W. M., and Koren, M. 1971, *Ap. J.*, **168**, 283; Erratum, **170**, 621.
Vaiana, G. S., Davis, J. M., Giacconi, R., Krieger, A. S., Silk, J. K., Timothy, A. F., and Zombeck, M. 1973, *Ap. J. (Letters)*, **185**, L47.
Vaiana, G. S., and Giacconi, R. 1969, in *Plasma Instabilities in Astrophysics*, ed. D. G. Wentzel and D. A. Tidman (New York: Gordon & Breach), p. 91.
Vaiana, G. S., Krieger, A. S., Silk, J. K., Timothy, A. F., Chase, R. C., Davis, J., Gerassimenko, M., Golub, L., Kahler, S., and Petrasso, R. 1974, in *IAU Symposium No. 56, Coronal Disturbances*, ed. G. Newkirk, Jr. (Dordrecht: Reidel), p. 501.
Vaiana, G. S., Krieger, A., and Timothy, A. F. 1973, *Solar Phys.*, **32**, 81.
Vaiana, G. S., Reidy, W. P., Zehnpfennig, T., Van Speybroeck, L. P., and Giacconi, R. 1968, *Science*, **161**, 564.
Vaiana, G. S., Van Speybroeck, L., Zombeck, M. V., Krieger, A. S., Silk, J. K., and Timothy, A. 1977, *Space Sci. Instr.*, in press.
Vorpahl, J. A. 1976, *Ap. J.*, **205**, 868.
Vorpahl, J. A., Gibson, E. G., Landecker, P. B., McKenzie, D. L., and Underwood, J. H. 1975, *Solar Phys.*, **45**, 199.
Waldmeier, M. 1974, in *IAU Symposium No. 57, Coronal Disturbances*, ed. G. Newkirk, Jr. (Dordrecht: Reidel), p. 149.
Webb, D. F., Krieger, A. S., and Rust, D. M. 1976, *Solar Phys.*, **48**, 159.
Widing, K. G. 1975, in *IAU Symposium No. 68, Solar Gamma-, X-, and EUV Radiation*, ed. S. R. Kane (Dordrecht: Reidel), p. 153.
Widing, K. G., and Cheng, C. C. 1974, *Ap. J. (Letters)*, **194**, L111.

R. PALLAVICINI: Osservatorio Astrofisico di Arcetri, Largo Fermi 5, 50125 Firenze, Italy

S. SERIO: Osservatorio Astronomico di Palermo, Palazzo del Normanni, Palermo, Italy

G. S. VAIANA: Harvard College Observatory, 60 Garden Street, Cambridge, MA 02138

PLATE 2

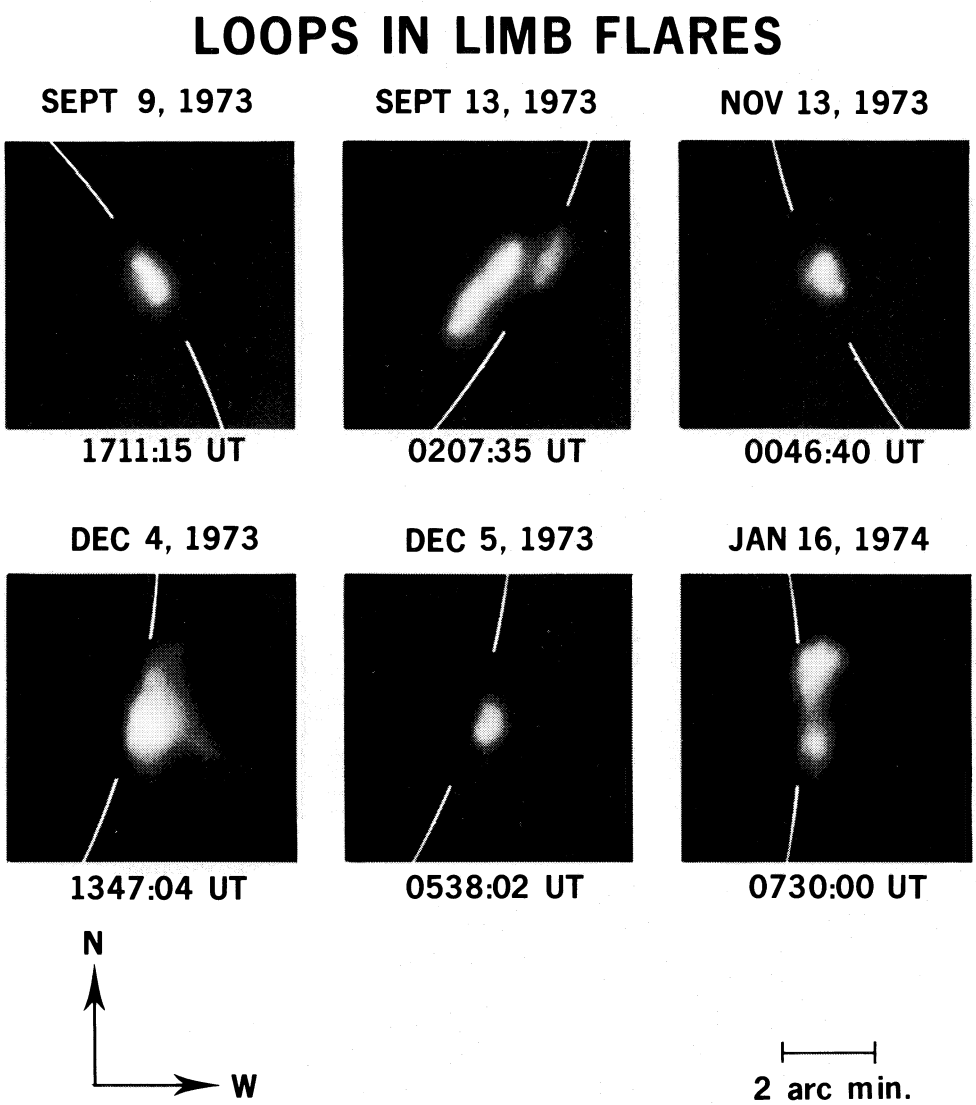

FIG. 1.—Examples of compact loops observed in X-ray limb flares. (*a*) September 9: filter 1, exposure time 4 s; (*b*) September 13: filter 1, exp. 4 s; (*c*) November 13: filter 1, exp. 4 s; (*d*) December 4: filter 5, exp. 64 s; (*e*) December 5: filter 5, exp. 16 s; (*f*) January 16: filter 3, exp. 0.3 s. White marks indicate the Sun limb.

PALLAVICINI *et al.* (*see* page 110)

POINT-LIKE LIMB FLARES

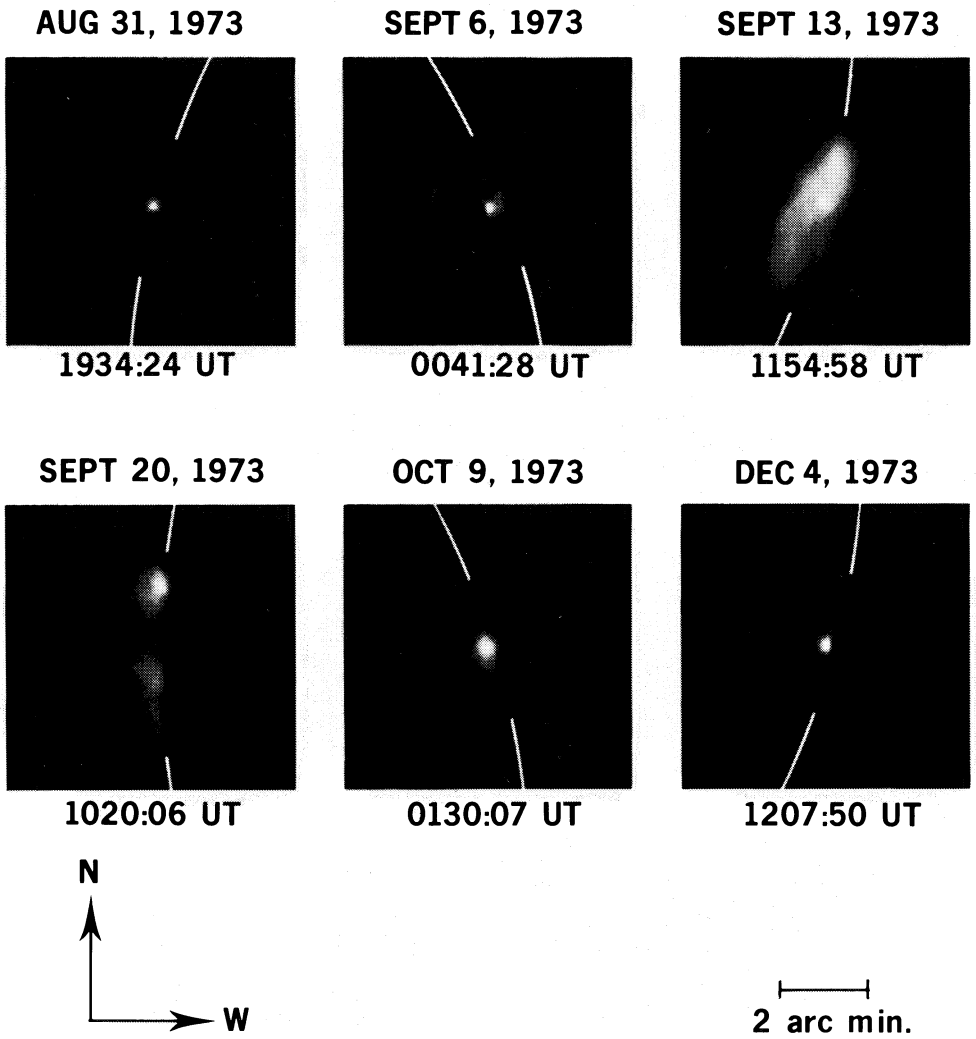

FIG. 2.—Examples of X-ray pointlike limb flares. (*a*) August 31: filter 1, exposure time 1/16 s; (*b*) September 6: filter 3, exp. 1/16 s; (*c*) September 13: filter 6, exp. 16 s; (*d*) September 20: filter 6, exp. 16 s; (*e*) October 9: filter 1, exp. 4 s; (*f*) December 4: filter 5, exp. 1/4 s. White marks indicate the Sun limb.

PALLAVICINI *et al.* (*see* page 110)

PLATE 4

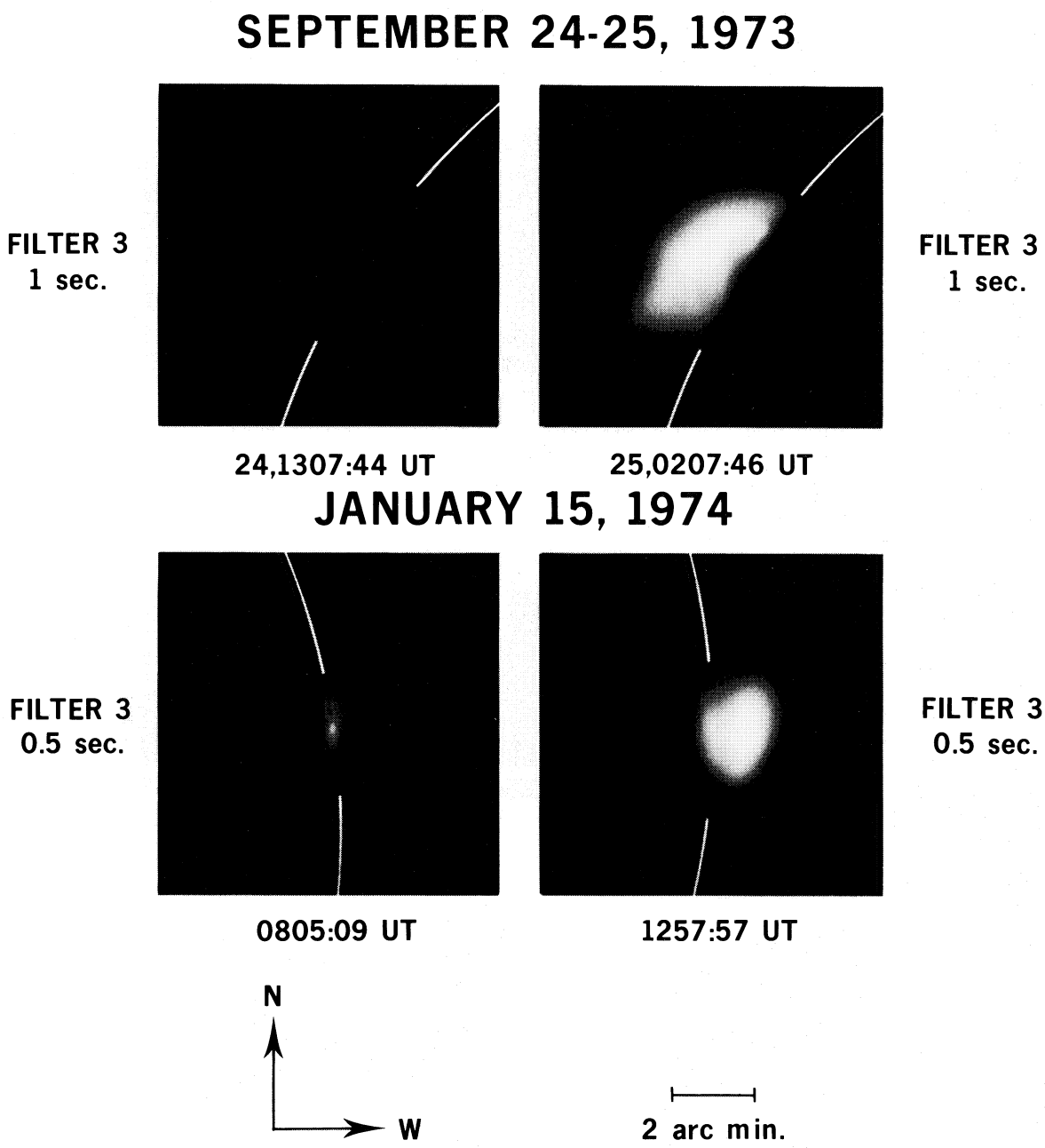

FIG. 3.—Two examples of X-ray limb flares with the development of large and diffuse systems of loops. For each event, an image taken during the decay phase of the flare is shown on the right-hand side of the figure. For comparison, an image taken with the same filter and with the same exposure time prior to the flare is shown on the left-hand side. White marks indicate the Sun limb.

PALLAVICINI *et al.* (*see* page 112)

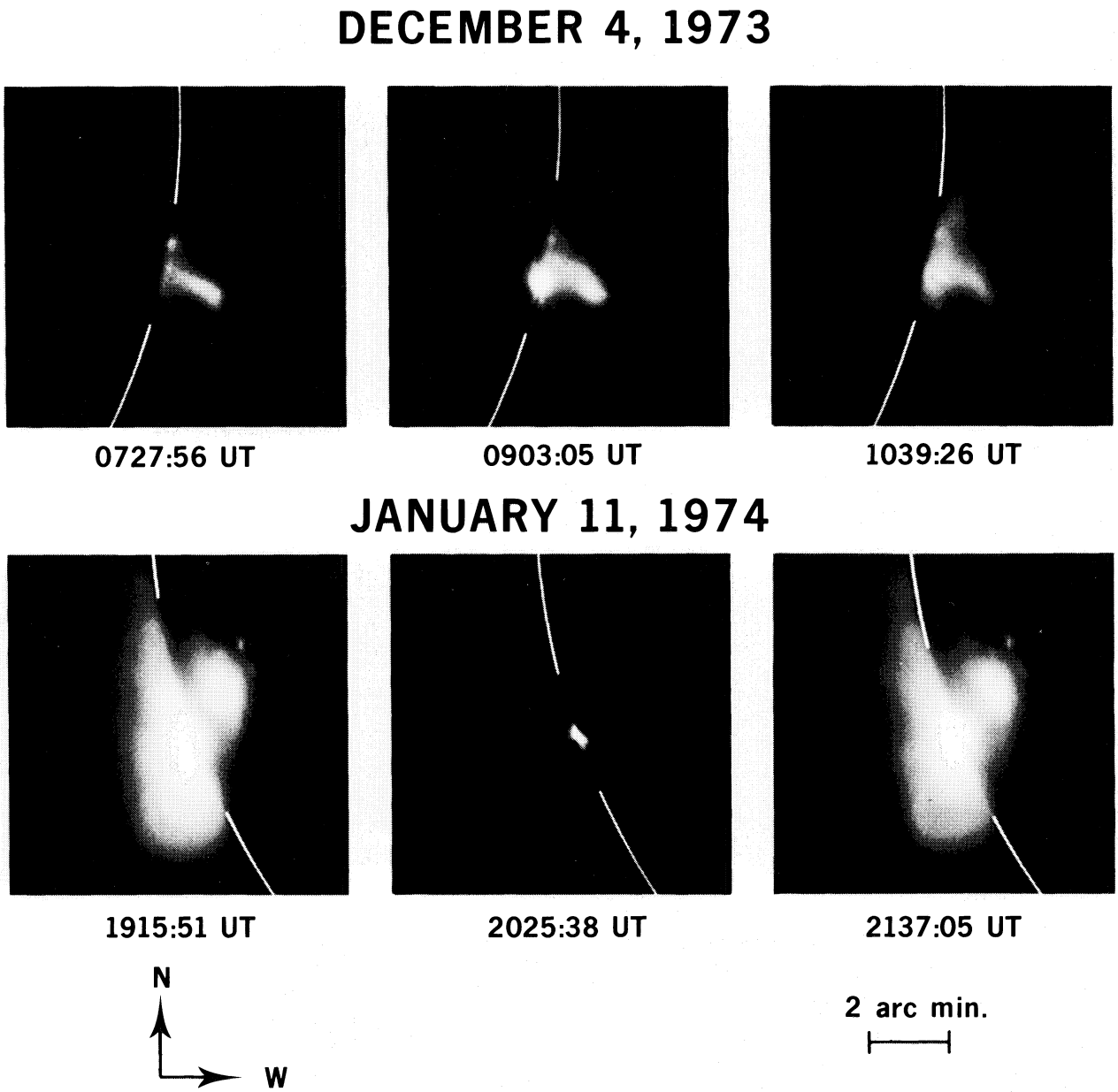

FIG. 4.—Two X-ray limb flares compared with the structure of the active region in the preflare and postflare phases. December 4: (*a*) 0727:56 UT (preflare), filter 5, exposure time 16 s; (*b*) 0903:05 UT (flare), filter 5, exp. 16 s; (*c*) 1039:26 UT (postflare), filter 5, exp. 64 s. January 11: (*d*) 1915:51 (preflare), filter 3, exp. 4.2 s; (*e*) 2025:38 (flare), filter 3, exp. 0.3 s; (*f*) 2137:05 UT (postflare), filter 3, exp. 4.2 s. The image at 2025:38 UT for the January 11 event is taken in the grating mode. White marks indicate the Sun limb.

PALLAVICINI *et al.* (*see* page 113)

PLATE 6

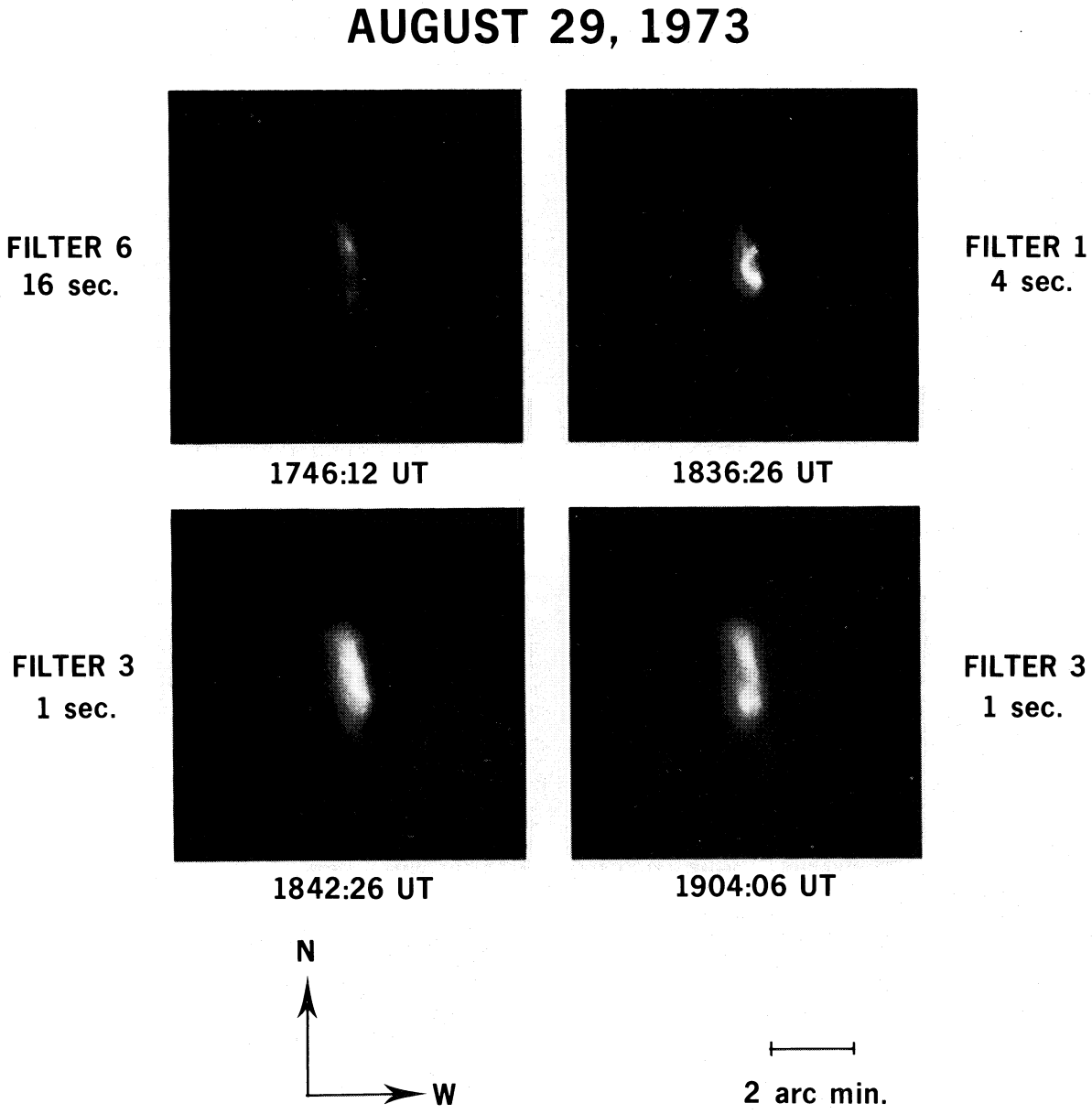

FIG. 5.—An X-ray event on 1973 August 29. The image at 1746:12 UT is taken during the preflare phase; the images at 1836:26 UT and 1842:26 UT are taken during the flaring period; the image at 1904:06 UT is taken in the postflare phase. Notice the bright loop during the flaring period.

PALLAVICINI *et al.* (*see* page 113)

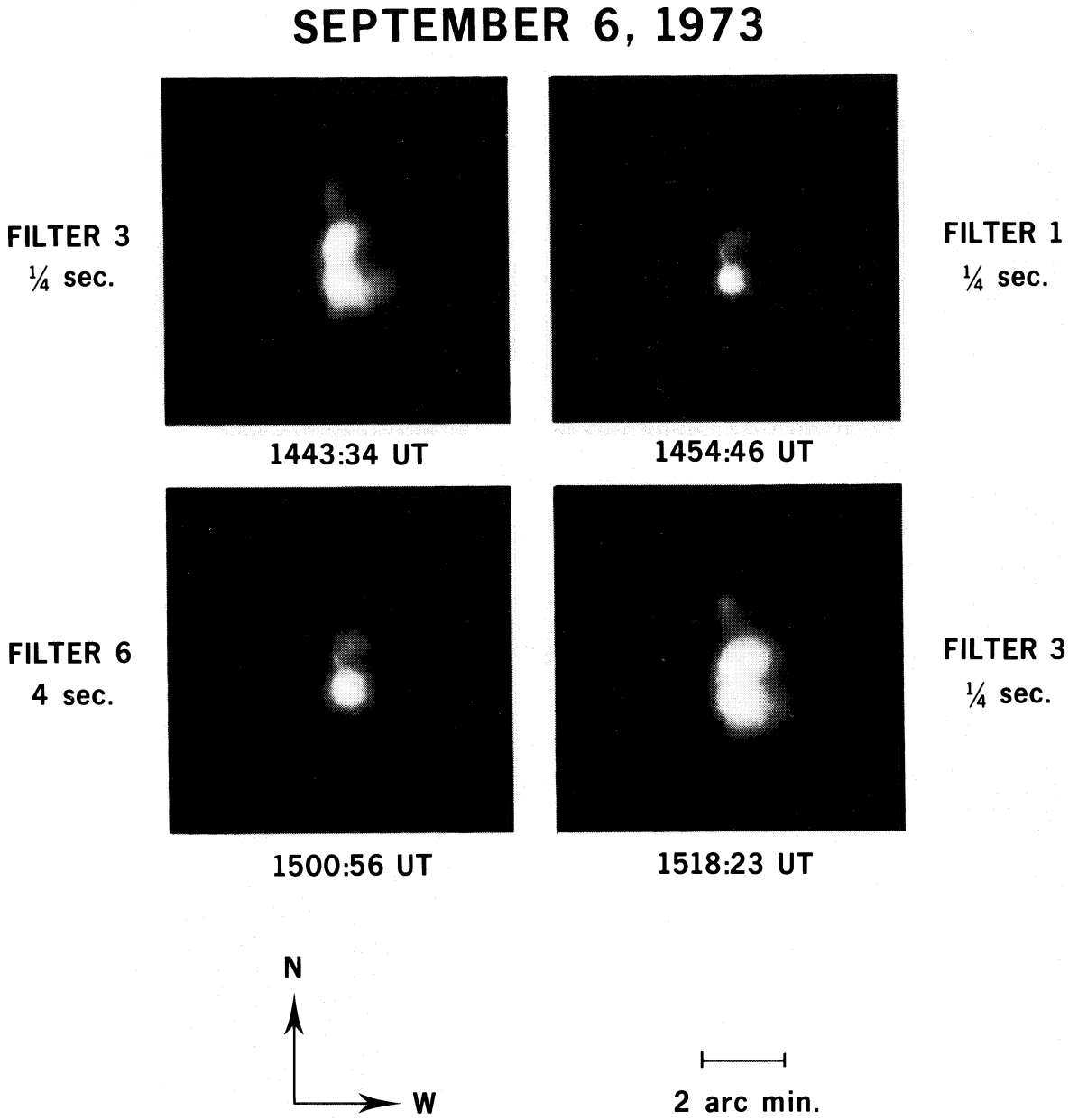

FIG. 6.—Temporal development of an X-ray event on 1973 September 6. The flare occurs at the base of the bright spikelike core of the active region visible toward the south in the image at 1443:34 UT. The location is the same as for the flare at 1220 UT discussed in the text (§ III).

PALLAVICINI *et al.* (*see* page 113)

PLATE 8

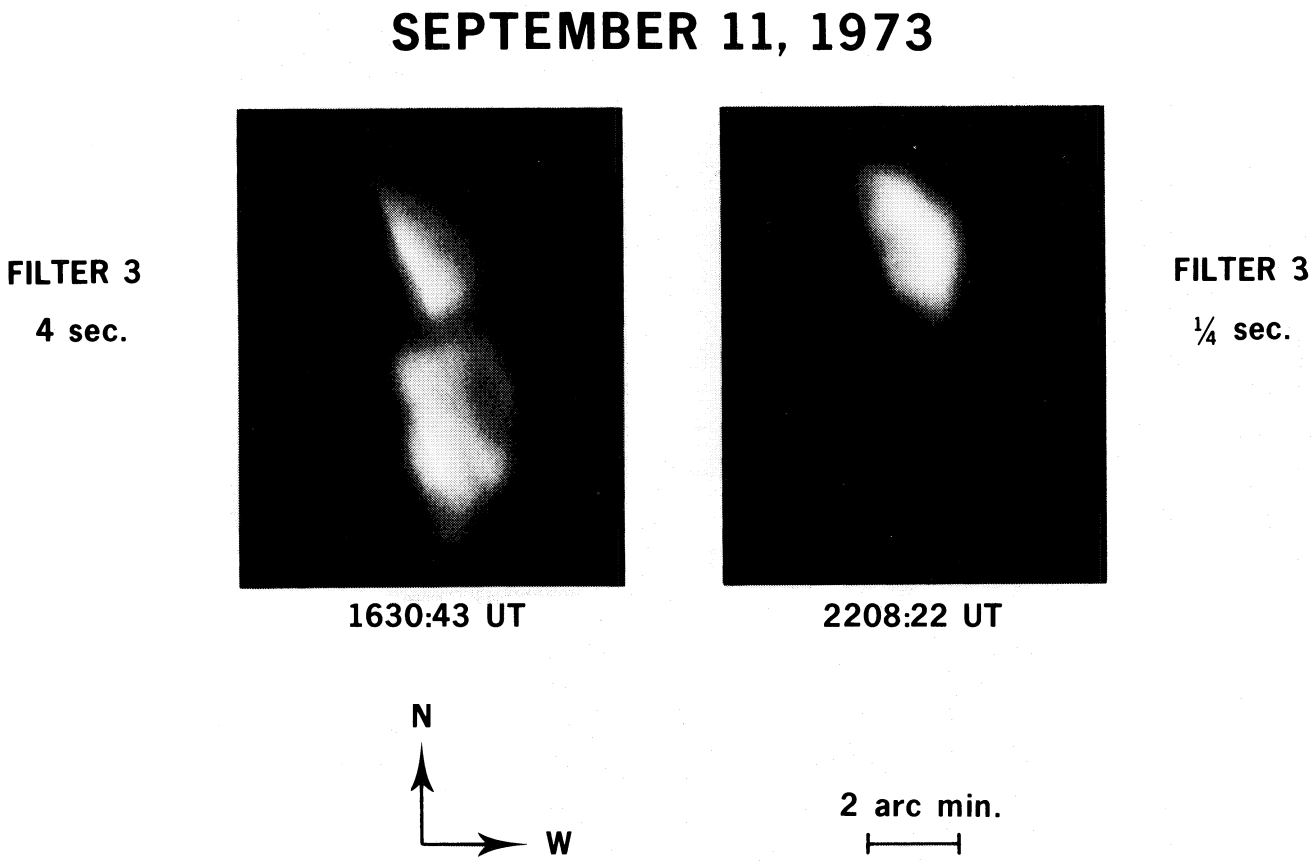

FIG. 7.—Comparison between an image taken at 2208:22 UT during the decay phase of a long-enduring X-ray event on 1973 September 11 and a preflare image taken at 1630:43 UT. The enhanced brightening of high systems of loops during the flaring period is more evident by comparison with the adjacent active region south of the flaring region. Notice the enhanced brightness at the top of the flaring loops.

PALLAVICINI *et al.* (*see* page 113)

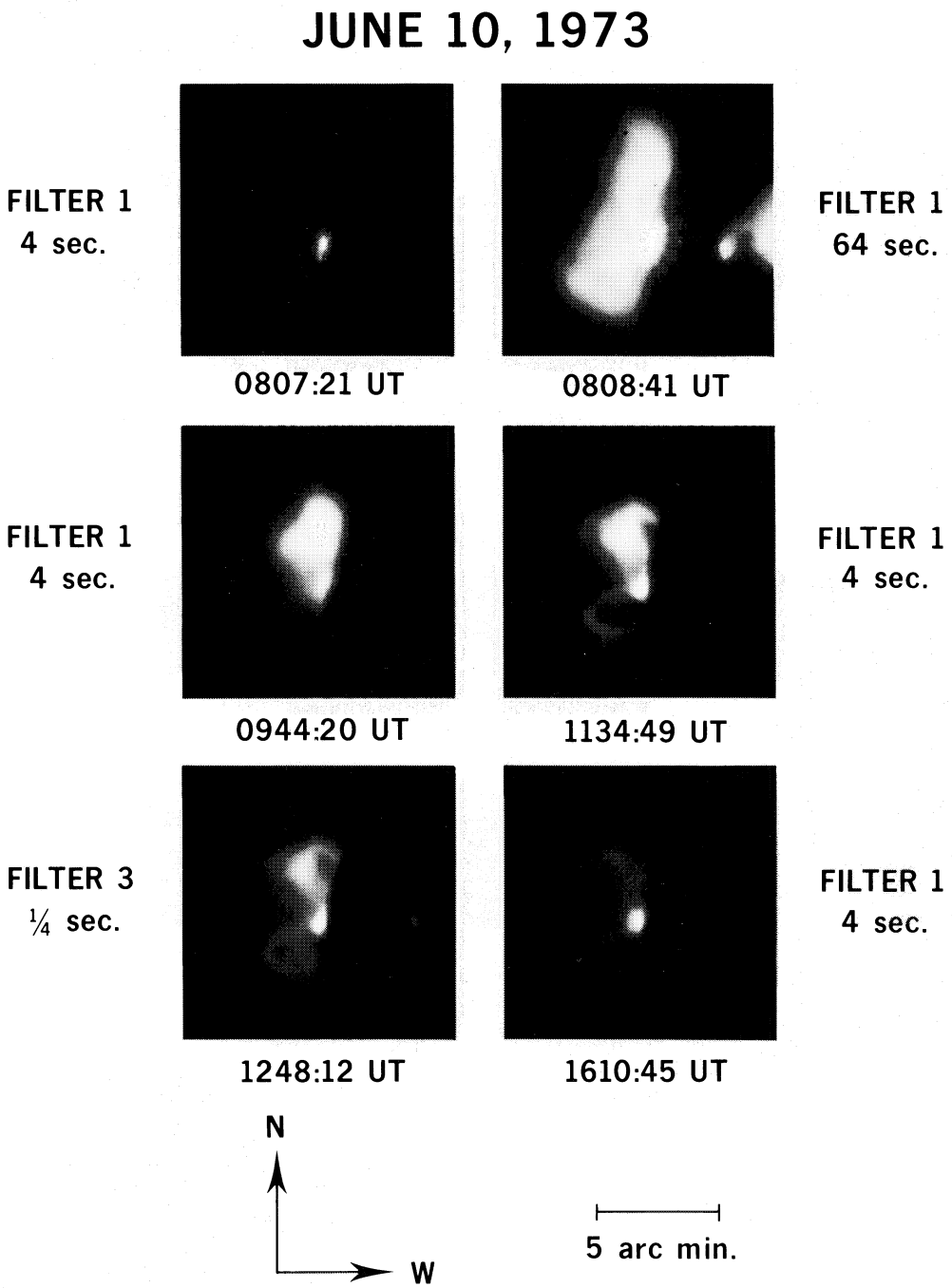

FIG. 8.—The temporal development of a long-enduring and complex X-ray event on 1973 June 10. Images at 0807:21 UT and 0808:41 UT are taken in the preflare phase during the late decay of a preceding event; the images at 0944:20 UT, 1134:49 UT, and 1248:12 UT are taken during the flaring period. The image at 1610:45 UT is taken in the postflare phase.

PALLAVICINI *et al.* (*see* page 113)